Geoscience Frontiers 12 (2021) 101187

HOSTED BY

Contents lists available at ScienceDirect

Geoscience Frontiers

journal homepage: www.elsevier.com/locate/gsf

Research Paper

Phosphorite generative processes around the Precambrian-Cambrian boundary in South China: An integrated study of Mo and phosphate O isotopic compositions

Haiying Yang [a,b], Jiafei Xiao [a,*], Yong Xia [a], Zhuojun Xie [a], Qinping Tan [a], Jianbin Xu [a,c], Shan He [a,d], Shengwei Wu [a,d], Xiqiang Liu [a,d], Xingxiang Gong [a,d,e]

[a] State Key Laboratory of Ore Deposit Geochemistry, Institute of Geochemistry, Chinese Academy of Sciences, Guiyang 550081, China
[b] School of Earth Sciences, Yunnan University, Kunming, 650500, China
[c] School of Qilu Transportation, Shandong University, Jinan 250061, China
[d] University of Chinese Academy of Sciences, Beijing 101408, China
[e] Reserve Bureau of Land and Mineral Resources of Guizhou Province, Guiyang 550081, China

ARTICLE INFO

Article history:
Received 30 November 2020
Revised 9 March 2021
Accepted 13 March 2021
Available online 3 April 2021

Handling Editor: C.J. Spencer

Keywords:
Doushantuo formation
Gezhongwu formation
Phosphorite
Ore-forming material origin
Phosphate O isotope
Mo isotope

ABSTRACT

Large phosphorite deposits in Central Guizhou, China, were formed around the Precambrian/Cambrian boundary (PC/C), including the Ediacaran (Doushantuo stage) and early Cambrian (Gezhongwu stage). Among them, Gezhongwu phosphorite from Zhijin are enriched in rare earth elements (REE) plus yttrium (REY), reaching 3.503 million tons. Although phosphorites have attracted great attention, the specific sources P and REY remained unclear. To determine the P and REY sources and establish a phosphogenic model of PC/C phosphorite, we present an integrated dataset of Mo and phosphate O isotopes for the first time, along with carbonate C and O isotopes, geology, petrology, and geochemistry. In all samples, $\delta^{18}O_p$, Y/Ho, and Zr/Hf decreased from the Ediacaran to the early Cambrian, indicating increased terrigenous weathering fluxes while decreased upwelling water input. Furthermore, terrigenous weathering delivery significantly elevated marine REY concentrations in the Cambrian in Zhijin. The Ce_{anom} and $\delta^{98/95}$Mo suggest that seawater was oxidized in the later Ediacaran and became entirely oxic in the early Cambrian. The positive feedback between oxygen levels in atmosphere and primary productivity caused progressive oxygenation in ocean–atmosphere system and enable phosphorites to be formed by different mechanisms. Results show that the Lower Doushantuo consist of abiotic intraclasts and exhibited "seawater-like" REY types, indicating abiological and mechanical reworking phosphogenesis. The Upper Doushantuo and Gezhongwu Formation contained mainly microbial debris and abiogenic intraclasts, and exhibit "hat-shaped" REY plots, suggesting microbially mediated phosphogenesis. Based on this data set, we developed a phosphogenic model illustrating formation of these two phosphorite deposits, wherein the Lower Doushantuo phosphorite formed through the reworking of pre-existing phosphatic sediments in anoxic and abiotic ocean, whereas the Upper Doushantuo and Gezhongwu phosphorite formed via microbial metabolisms in oxic and biotic conditions. Our study has implications on the PC/C phosphorite generative processes, as well as paleoenvironmental conditions.

1. Introduction

Phosphorus is a prime element in Earth's history because of its ability to reconstruct long-term feedback mechanisms among climate, environment, ecology, and global change. The first major worldwide phosphogenic events began in the Cryogenian and ended in the Cambrian (Cook and Shergold, 1984; Cook, 1992), associated with the Neoproterozoic Oxygenation Event (Och and Shields-Zhou, 2012). Marine sedimentary phosphorite in South China mainly formed around the Precambrian/Cambrian boundary (PC/C) (~541 Ma) and accounts for more than 80% of all phosphorite resources in China. The South China develop complete stratigraphic sequence, especially phosphorite strata of Ediacaran and Early Cambrian, it is a perfect location to unravel the phosphogenesis enigma. Both the well-known Doushantuo phosphorites of the

* Corresponding author.
E-mail address: xiaojiafei@vip.gyig.ac.cn (J. Xiao).

https://doi.org/10.1016/j.gsf.2021.101187

Ediacaran and Gezhongwu phosphorites of the Cambrian are distributed in Central Guizhou (Fig. 1) (Shu, 2012). Ediacaran phosphorite deposits are located in the Weng'an County with high P content and negligible REY concentrations, while Cambrian phosphorite deposits are located at Zhijin County with rich P and REE resources.

PC/C-age phosphorites in South China are well-known and have been well-studied. The origin of ore-forming materials is the key information to reveal the generative processes of phosphorite deposits. The prevailing paradigm suggests that the ore-forming materials of the PC/C phosphorite were derived from the weathering of terrestrial materials (Föllmi, 1996; Filippelli, 2008; Planavsky et al., 2010; Shimura et al., 2014; Pufahl and Groat, 2017; Yang et al., 2019). Another origin of phosphorite deposits in this region is the upwelling events transporting P-rich waters from the deep sea (Liu et al., 1987; Glenn et al., 1994; Jarvis et al., 1994; Mi, 2010), which is supported by petrographic evidence (Liu et al., 1987; Mi, 2010) and stable carbon isotopes (Lambert et al., 1987; Jiang et al., 2007). Furthermore, hydrothermal fluids have also been considered as potential sources because of the "hat-shaped" post-Archean Australian shale (PAAS)-normalized REY distributions, positive Eu anomalies, Fe-Mn-(Ni + Co + Cu) ternary diagrams (Shi et al., 2004; Shi, 2005; Guo et al., 2017; Yang et al., 2019), and the tubular and alveolate eruption throats in Weng'an deposits (Guo et al., 2003). Past studies on the sources of Guizhou phosphorites have been focused on the petrographic and geochemical characteristics of bulk rock samples, which can record the traits of ore-forming materials to a certain degree. Although the viewpoints about the ore-forming materials of the PC/C phosphorite are well studied, the source/s of P remains

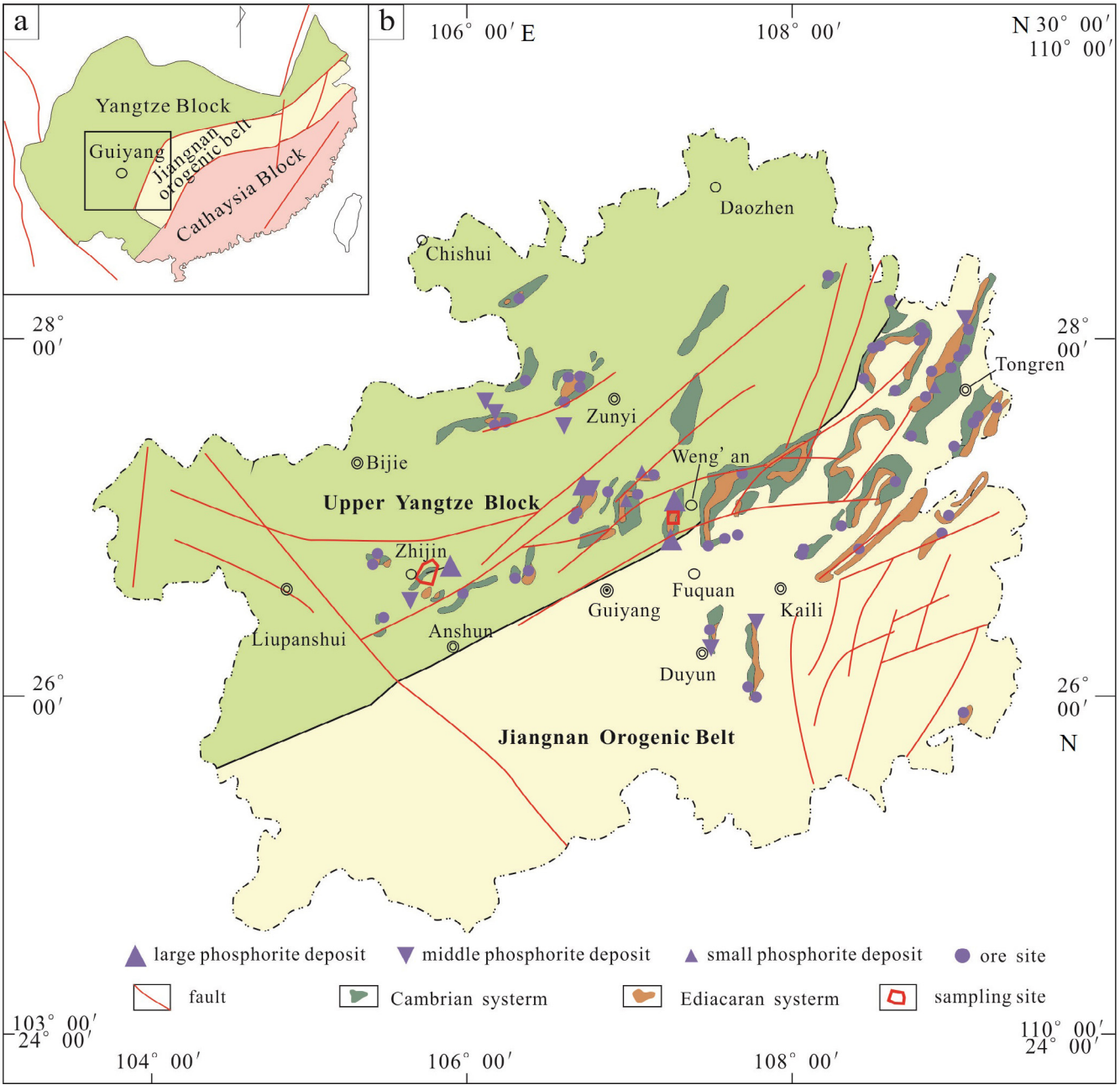

Fig. 1. Tectonic sketch map of Guizhou and distribution of phosphorites: (a) after Shu (2012); (b) after Wu et al. (1999).

controversial, and that of REE were poorly studied. Studies confirming the specific source(s) of P and REY are necessary to reveal the phosphorite formation.

Phosphorus is only pentavalent without stable isotopes and exists as nearly stable tetrahedra when combined with oxygen. In addition, once the phosphate precipitated or apaptite formed, the oxygen was locked in the apatite and did not likely alter during diagenesis (Blake et al., 2010; Jaisi and Blake, 2010; Liang and Blake, 2007). Hence, the oxygen isotope of phosphate ($\delta^{18}O_p$) value is useful indicators of the origins of P in sedimentary systems (Blake et al., 2005; Colman et al., 2005; McLaughlin et al., 2006; Young et al., 2009). Recently, their importance for tracing water contamination by fertilizers and soils (Gruau et al., 2005; Young et al., 2009) and for P origins in phosphate sediments (Jaisi and Blake, 2010; Yuan et al., 2019) have received much attention. In the past decades, Michael Bau and colleagues had conducted a lot of researches of Y and Ho differentiation in aqueous (Bau et al., 1995), hydrothermal (Bau and Dulski, 1995, 1999), magmatic (Bau, 1996), and metamorphic (Bau and Möller, 1992) systems, indicating that the Y/Ho and Z/Hf ratios of different systems are obviously discrepant (Bau, 1996). The Y/Ho and Z/Hf ratios were commonly used to trace origins (Zhao et al., 2013; Xin et al., 2015) due to the significant difference between different sources. Here, we conduct a combined data including $\delta^{18}O_p$, Y/Ho, and Zr/Hf, aiming to ascertain the source(s) of P and REY.

Redox conditions are considered as important factors during phosphorite formation, and many previous geochemical studies have focused on the redox conditions of PC/C phosphorites. It is now widely known that there was redox stratification in the South China ocean near the PC/C boundary according to the $\delta^{13}C_{org}$, $\delta^{13}C_{carb}$, and Mo, Fe, and S isotopes (Goldberg et al., 2007; Jiang et al., 2007; Canfield et al., 2008; Wille et al., 2008; Han and Fan, 2015). Following that, the shallow water on the Yangtze Platform was completely oxygenated during the early Cambrian (Fan et al., 2016; Liu, 2017). Phosphate mineralization occurred near the redox interface (Canfield et al., 2007; Fike and Grotzinger, 2008; Wille et al., 2008) through Fe-pumping (Canfield et al., 2007; Jiang et al., 2011). Although considerable progress has been made in revealing the redox conditions during the Ediacaran-early Cambrian phosphorite formation, there have been few studies interpreting the role of the redox conditions taken in the formation of phosphorite near the PC/C boundary and in the REY-rich processes during Gezhongwu stage.

Ce anomalies and Mo isotopes of phosphorites have been used to reveal the redox evolution, for that cerium was redox-sensitive trace element and established as a redox indicator (Shimizu and Masuda, 1977; Wang et al., 1986; Murray et al., 1990; Shields and Stille, 2001), as well as Mo isotopes (Crusius et al., 1996; Morford and Emerson, 1999). The general geochemistry of Mo is widely discussed (Crusius et al., 1996; Morford and Emerson, 1999; Kendall et al., 2017) as a redox-sensitive trace metal in many geological processes. In the past years, Mo isotopes of euxinic sediments were used to reflect the seawater isotopic compositions (Arnold et al., 2004; Nägler et al., 2011; Noordmann et al., 2015). Voegelin et al. (2009) proposed for the first time that non-euxinic sediment (marine carbonate) show potential to record the Mo isotopic composition of ancient seawater. And the Mo isotope of phosphorite were applied to reflect the redox conditions of Cambrian seawater in South China (Wen et al., 2010, 2011; Liu, 2017). Here, we conducted Ce anomies of all samples and the Mo isotopic compositions of Weng'an phosphorite, combining with Mo isotopic compositions of the Zhijin phosphorite reported by Liu (2017), to reveal the redox evolution from Ediacaran to early Cambrian.

At present, several phosphorite formation processes have been proposed, including the reworking of previous phosphate deposits (Föllmi, 1996; Ilyin, 1998; Yang et al., 2019; Zhang et al., 2019), in situ diagenetic mineralization driven by changes in pore water redox potential (Frohlich et al., 1983; Föllmi, 1996; Pufahl and Hiatt, 2012; Muscente et al., 2015), abiogenic accretion (She et al., 2013, 2014; Yang et al., 2019), microbial breakdown of buried organic matter (OM) (Föllmi, 1996), and hydrothermal precipitation (Guo et al., 2003; Shi, 2005; Deng et al., 2015). Even though the formation processes have been widely discussed and several models for the formation of phosphorites in South China were proposed, there remains no complete and consecutive phosphogenic model for the Ediacaran-early Cambrian marine phosphorites of South China combined the sources, redox evolutions, and formation processes.

Previous studies have not resolved the specific source(s) of P and REY, and failed to connect redox evolution and formation mechanism. Here, we firstly report a new data combining Mo and phosphate O isotopes, along with comprehensive dataset including geological, petrographic, and geochemical characteristics and carbonate C, O isotopes for the Weng'an and Zhijin deposits. With these new data, we aim to trace the specific sources of P and REY, constrain the redox evolution, reveal the generative process/es of the phosphorite, and establish the phosphogenic model of the phosphorite formations. Integrated analyses of the petrology and geochemistry of Ediacaran to early Cambrian phosphorite may allow for a holistic understanding of the PC/C phosphorite formation in South China, during which the Neoproterozoic geodynamic events are suggested as triggers for increased weathering, upwelling, radiation of metazoans, and phosphogenesis.

2. Geological setting

2.1. Regional geology

The Yangtze Block and the Cathaysia Block joined together during Jinningian tectonics (0.9–0.82 Ga), resulting in the ancient South China Plate and formation of the Jiangnan Orogenic Belt (Shu, 2012; Zhang et al., 2013). The NW side of the Jiangnan Orogenic Belt is the Yangzte Block, and the SE side is the Cathaysia Block, which forms the basic tectonic framework of South China. Subsequently, the Yangtze and Cathaysia blocks underwent multiple tectonic movements along with the fragmentation and breakup of the Rodinia Supercontinent in the early Neoproterozoic era, leading to a series of graben–horst sub-basins along the SE margin of the Yangtze Block (Jiang et al., 2003; Wang and Li, 2003; Zhang et al., 2013). In the Ediacaran, the South China Plate underwent steadier break-up of supercontinents (Dong Ye, 1996; Wang and Li, 2003; Zhang et al., 2013), while the Jiangnan Orogenic Belt persisted as a series of submarine highlands (Dong Ye, 1996). During the Cambrian period the paleographic framework of South China was similar to that during the Neoproterozoic, with the water deepening from the NW platform toward the SE ocean basin (Liu et al., 1993). The lithofacies deposited in South China developed continental, neritic, and abyssal clastic rocks, as well as deep sea siliceous rocks from NW to SE (Liu et al., 1993; Xue et al., 2001).

Ediacaran to early Cambrian successions are well preserved in the Yangtze Platform. In the Ediacaran, Zhijin and Weng'an shows a carbonate platform (Fig. 2a) (Shen et al., 1998), with open shallow water and preserving shallow-water sediments (Wang et al., 2016). The Ediacaran successions in Weng'an are represented by Doushantuo Formation and overlying Dengying Formation. In the early Cambrian, the seawater deepened in Central Guizhou, and transitional environments between the platform and protected basin were recorded in Zhijin and Weng'an (Fig. 2b) (Steiner et al., 2001). The early Cambrian successions in Zhijin are

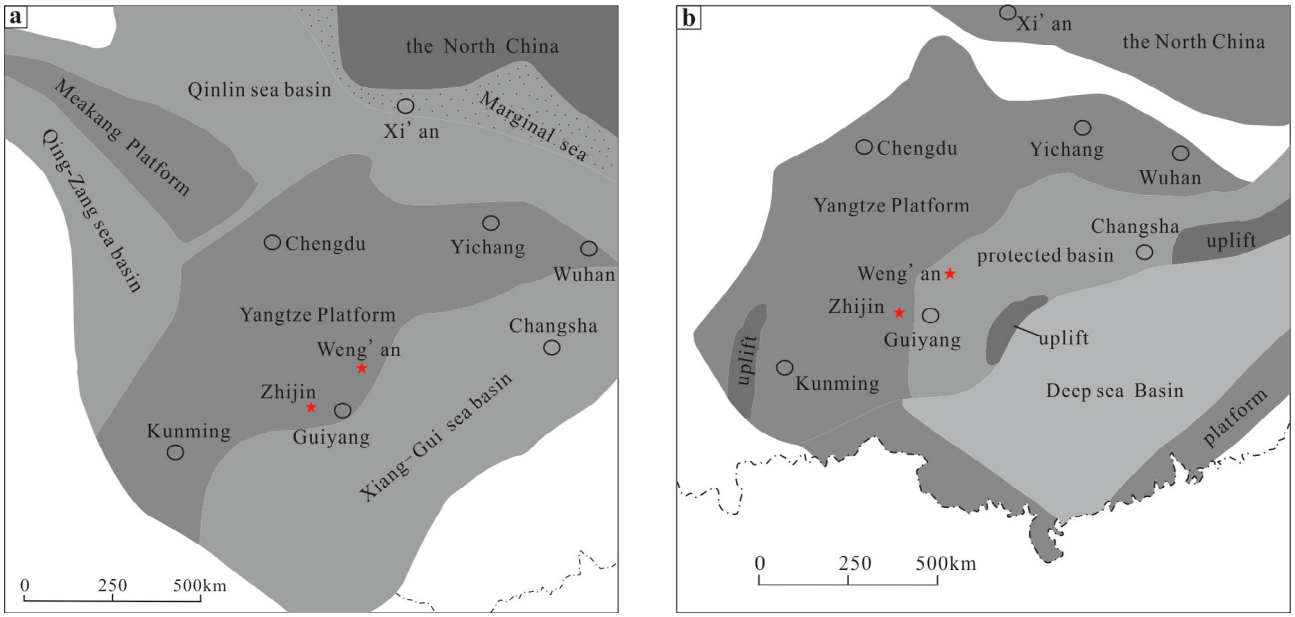

Fig. 2. Simplified palaeogeographic maps of the Yangtze Platform during (a) Ediacaran (from Shen et al., 1998)) and (b) Cambrian (from Steiner et al., 2001).

represented by Gezhongwu Formation and overlying Niutitang Formation.

2.2. Ore deposit geology

2.2.1. Strata and tectonics

The exposed strata in the Weng'an deposits mainly consist of the Banxi Group of the Qingbaikou system (Ptb*n*), Nanhuan Member of the Nantuo Formation (Nh*n*), the Doushantuo and Dengying formations of the Sinian (~Ediacaran in geological age) sequence (Z*d*), Cambrian, Permian, and Triassic system (Fig. 3a). Among them, phosphorites occur in the Doushantuo Formation, which unconformably overlies the Nantuo tillite and conformably underlies the Dengying carbonates. The Doushantuo Formation in Weng'an may be divided into four members, the lithologies of which can be described as follows (Fig. 3b): the Z_1d^1 layer is composed of dolomite with cross-bedding, horizontal bedding, and microscale wavy bedding; Z_1d^2 (Lower Doushantuo) is a thin-to-medium-thickness ore body consisting of off-white siliceous phosphorite, with parallel and horizontal bedding; Z_1d^3 is composed up of dolomite, siliceous dolomite, and chert, with bioturbation; Z_1d^4 (Upper Doushantuo) is a medium ore body consisting of dolomitic phosphorite and abundant microbial debris. Phosphorite occurs in Z_1d^2 and Z_1d^4 layers, with dolomites serving as wall rocks. The Baiyan–Gaoping Anticline is the most critical ore-controlling tectonic structure and is crossed by the N–S-trending Xiaoba Fault. This intersection resulted in the NE-trending Baiyan Anticline and NNE-trending Gaoping Anticline, which provides the basic framework of the Weng'an deposits (Fig. 3a). These anticlines control the NE-trending distribution of phosphorites, as well as other strata.

In the Zhijin deposit, the exposed strata mainly consist of those from the Doushantuo and Dengying formations of the Sinian (Z*d*), Cambrian, Devonian, Carboniferous, Permian, and Triassic systems (Fig. 4a). Phosphorite occurs in the Gezhongwu Formation, the lower Cambrian series, and unconformably overlies the carbonates of the Dengying Formation and conformably underlies the sandy shale of the Niutitang Formation. Both the Dengying and Niutitang formations served as country rocks. The Gezhongwu Formation was divided into two members, the lithologies of which are described as follows (Fig. 4b): ϵ_1gz^1 (Lower Gezhongwu) is composed of dolomitic phosphorites, with parallel and cross-bedding; ϵ_1gz^2 (Upper Gezhongwu) consists of striped siliceous phosphorite with wavy bedding. The main ore-controlling faults, the Guohua–Gezhongwu Fault (F_1) and Guiguo–Damachang Fault (F_2), spread toward the NE, and are located at the center of the Guohua–Gezhongwu Anticline (f_1) and Guiguo–Damachang Anticline (f_2), respectively (Fig. 4a). Synclines are developed between the anticlines and numerous NE-trending faults developed, including strike-slip, reverse, and normal faults. The primary tectonics and derived faults have caused the strata to trend NE and banded exposures along with the Guohua–Gezhongwu and Guiguo–Damachang anticlines.

2.2.2. Ore bodies

The phosphorite "ore bodies" refers to the geologic bodies that have mining value and contain sufficient phosphate ore. The Weng'an ore bodies are stratabound and occur in the Z_1d^2 and Z_1d^4 layers (Fig. 3b). Ore bodies are exposed and spread toward the NNE along with the wings and cores of the Baiyan and Gaoping anticlines, with P resources reaching 0.794 billion tons. The deposit was divided into the Baiyan and Gaoping mining districts. The Baiyan mining area is 11 km in length and 2.5–3 km in width, with an acreage of 28 km^2, including the Xiaoba, Yingping, Mofang, and Dazhai ore blocks (Fig. 3a). The Gaoping mining area is 9 km in length and 3–3.5 km in width, with an acreage of 30 km^2, including the Yuhua, Wangjiayuan, Datang, and Chuyandong ore blocks (Fig. 3a).

The Zhijin ore bodies are also stratabound and occur in the Cambrian Gezhongwu Formation (Fig. 4b). Ore bodies spread toward the NE along with the cores of the anticline, with 3.39 billion tons of P ore resources. Moreover, according to "Investigation Report of Phosphorite (rare earth) Ore in Zhijin Area, Guizhou Province" provided by Bureau of Geology and Mineral Exploration and Development of Guizhou Province, the REY resources (RE_2O_3) are enriched in the Zhijin phosphorites, reaching 3.503 million tons with an average grade of 0.1036%. The Zhijin deposit, with an acreage of 333 km^2, was divided into the Xinhua Mining District on the northwestern side and the Damachang Mining District on the southeastern side. The mineral resources are mainly from the

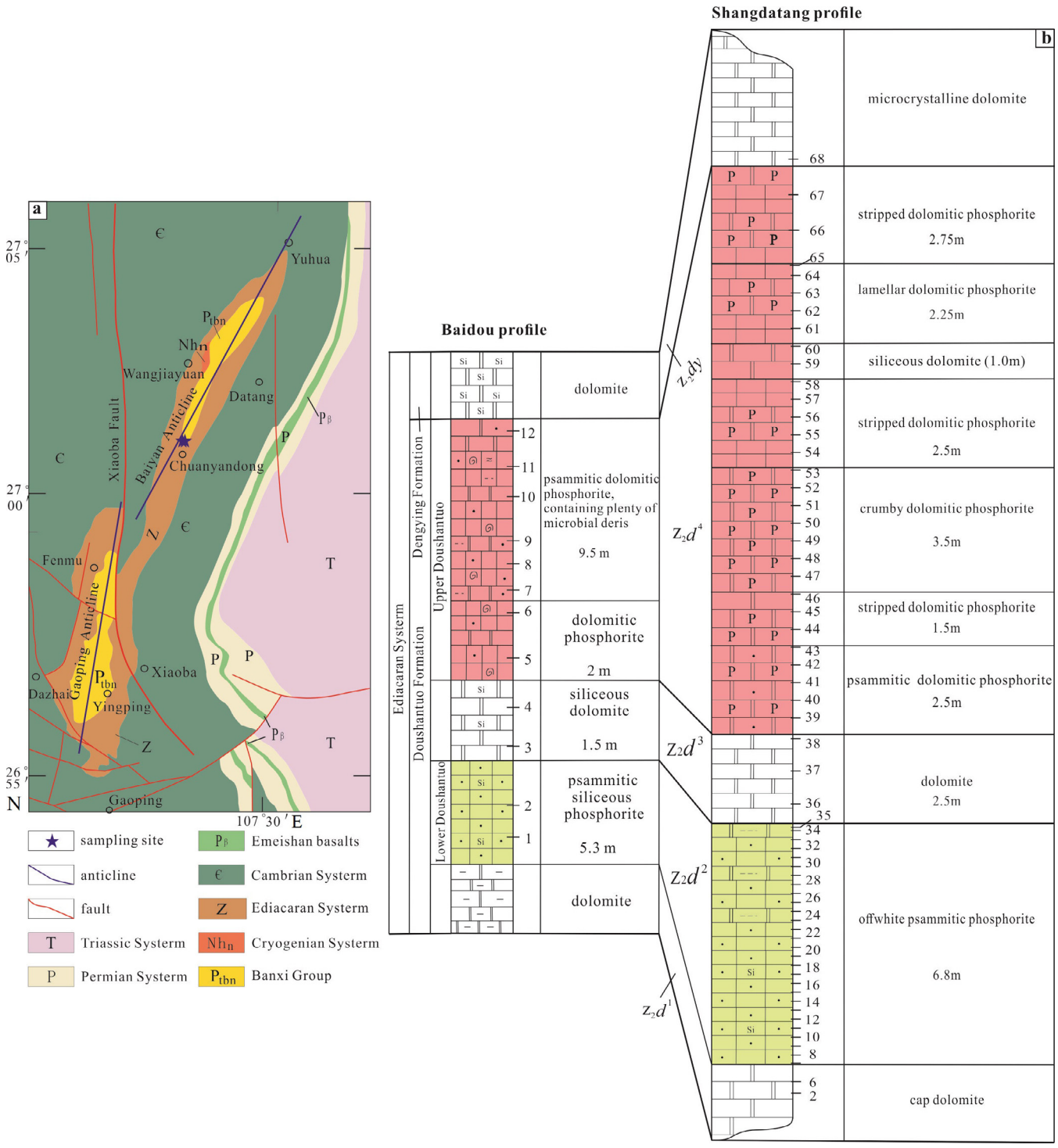

Fig. 3. (a) Tectonic setting of Weng'an phosphorite deposits; (b) simplified stratigraphic columns and sampling locations of the Shangdatang and Baidou profiles in Weng'an.

Xinhua Mining District, including the Daga, Motianchong, Guohua, Ganjiayakou, Gezhongwu, and Gaoshan ore blocks (Fig. 4a).

2.2.3. Mineralogy

The phosphorites examined in this study can be classified into different types according to their sedimentary structures, including banded (Fig. 5a, b), striped (Fig. 5c), massive (Fig. 5d), brecciated (Fig. 5e), spherulitic (Fig. 5f), psammitic (Fig. 5g), and broken (Fig. 5h) structure. The Lower Doushantuo consists of banded and massive phosphorites with psammitic mineral grains, developing horizontal bedding (Fig. 5i). The Upper Doushantuo has the most complicated structures, including brecciated, spherulitic, broken, and crumbling structures, with abundant spherulitic microbial debris and crumbled quartz (Fig. 5j). The Lower Gezhongwu has massive phosphorites consisting of psammitic and silty mineral grains. The banded and striped structures, consisting of off-white phosphatic dolomite bands and black dolomitic phosphorite bands, are mainly distributed in the Upper Gezhongwu. The Gezhongwu Formation exhibits parallel (Fig. 5k), cross-, and wavy bedding (Fig. 5l).

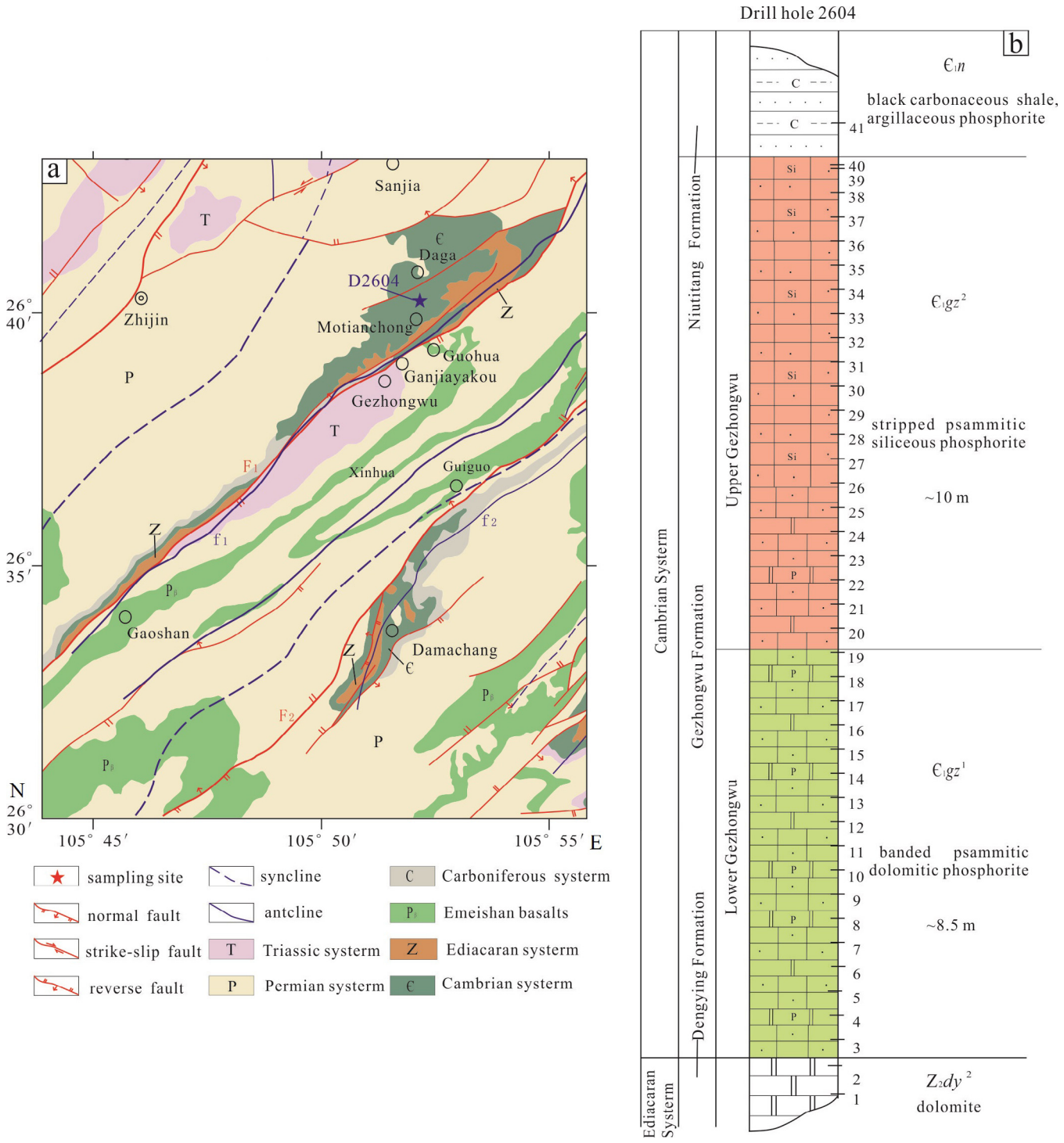

Fig. 4. (a) Tectonic setting of Zhijin phosphorite deposits; (b) simplified stratigraphic columns and sampling locations of Drill Core 2604 in the Motianchong ore block, Zhijin.

Rocks from the two-stage ore blocks have simple mineral compositions. Ore minerals occur dominantly as collophane, and gangue minerals mainly include dolomite, calcite, quartz, pyrite, chalcopyrite, and K-feldspar. The collophane of the Lower Doushantuo is composed of globular intraclasts in close contact with each other. The globular intraclasts have stable diameters of approximately 200–300 μm, are round, elliptical, or spindly (Fig. 6a), and contain quartz or dolomite. Partial intraclasts have developed isopachous shells and even have oolitic structures (Fig. 6a). The Lower Doushantuo developed many octahedral pyrites (Fig. 6b), 10–80 μm in diameter. The bottom of the Upper Doushantuo is mainly irregular blocky phosphate (Fig. 6c), cemented with dolomite. The Upper Doushantuo consists of almost microbial debris with a highly variable diameter size ranging from 50 μm to 2 mm. The microbial debris includes algal-like (Fig. 6d) and embryo-like (Fig. 6e) microfossils. All the algal-like microfossils are 200–600 μm in diameter, globular, and composed of cuboidal cell-like packets (Fig. 6d). The embryo-like microfossils are 100–400 μm in diameter, appear as globular, and comprise an inner core and isopachous cement with a thickness of 10 μm

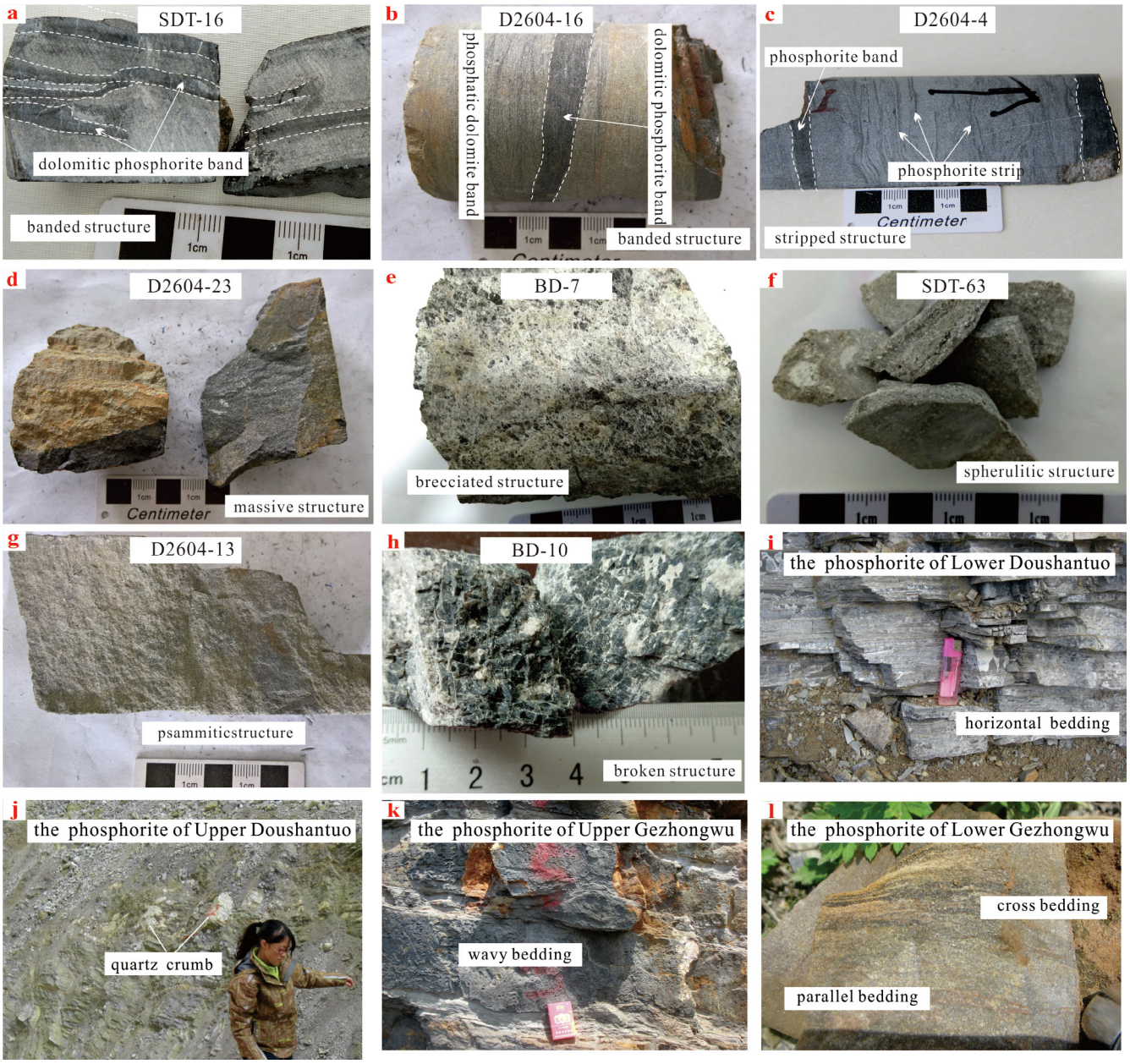

Fig. 5. Structural characteristics of phosphorites from the Ediacaran Doushantuo Formation and Cambrian Gezhongwu Formation in Central Guizhou. Abbreviations: SDT, samples from the Shangdatang profile in Weng'an; BD, samples from the Baidou profile in Weng'an; D, samples from the Motianchong drill hole in Zhijin.

(Fig. 6e). The amorphous apatite (Fig. 6e, h) cemented with dolomite in random morphologies, which were found among microbial debris. Additionally, shrinkage cracks, spongy textures, and isopachous cement were observed in almost all globular phosphate intraclasts, which were described in detail in our previous study (Yang et al., 2019). The Upper Doushantuo developed hematite (Fig. 6f), which might be oxidative products of magnetite.

The collophane of Zhijin can be classified into abiogenic intraclasts (Fig. 6g–i) and microbial debris (Fig. 6j–l). The abiogenic intraclasts have smaller diameters ranging of ~20–200 μm and exhibit globular (Fig. 6g), metasomatic (Fig. 6h), and irregular forms (Fig. 6i). The metasomatic form resulted from the metasomatism of phosphate intraclasts by quartz or dolomite. The microbial debris who were supposed small shelly organisms, displays multiple shapes under a scanning electron microscope (SEM), including columnar (Fig. 6j), peloidal (Fig. 6k), and dentiform (Fig. 6l). Most of the microbial debris were arranged directionally among the dolomite and were obviously bounded by the dolomite. Both abiogenic intraclasts and microbial debris are distributed throughout the section, while the collophane content in the Lower Gezhongwu was significantly higher than that of the Upper Gezhongwu. The cement of the Lower Gezhongwu was mainly dolomitic whereas that of the Upper Gezhongwu was mainly quartzose and dolomitic. The quartz and clay minerals increase from the bottom to the top of the section.

3. Materials and methodologies

Fieldwork undertaken in this study included in situ sampling in Weng'an and drill hole sampling in Zhijin. A total of 121 samples were collected, consisting of 80 samples from the Baidou (BD) and Shangdatang (SDT) profiles of the Weng'an deposits (Fig. 3b, blue stars), and 41 samples from drill hole 2604 (D2604) in the

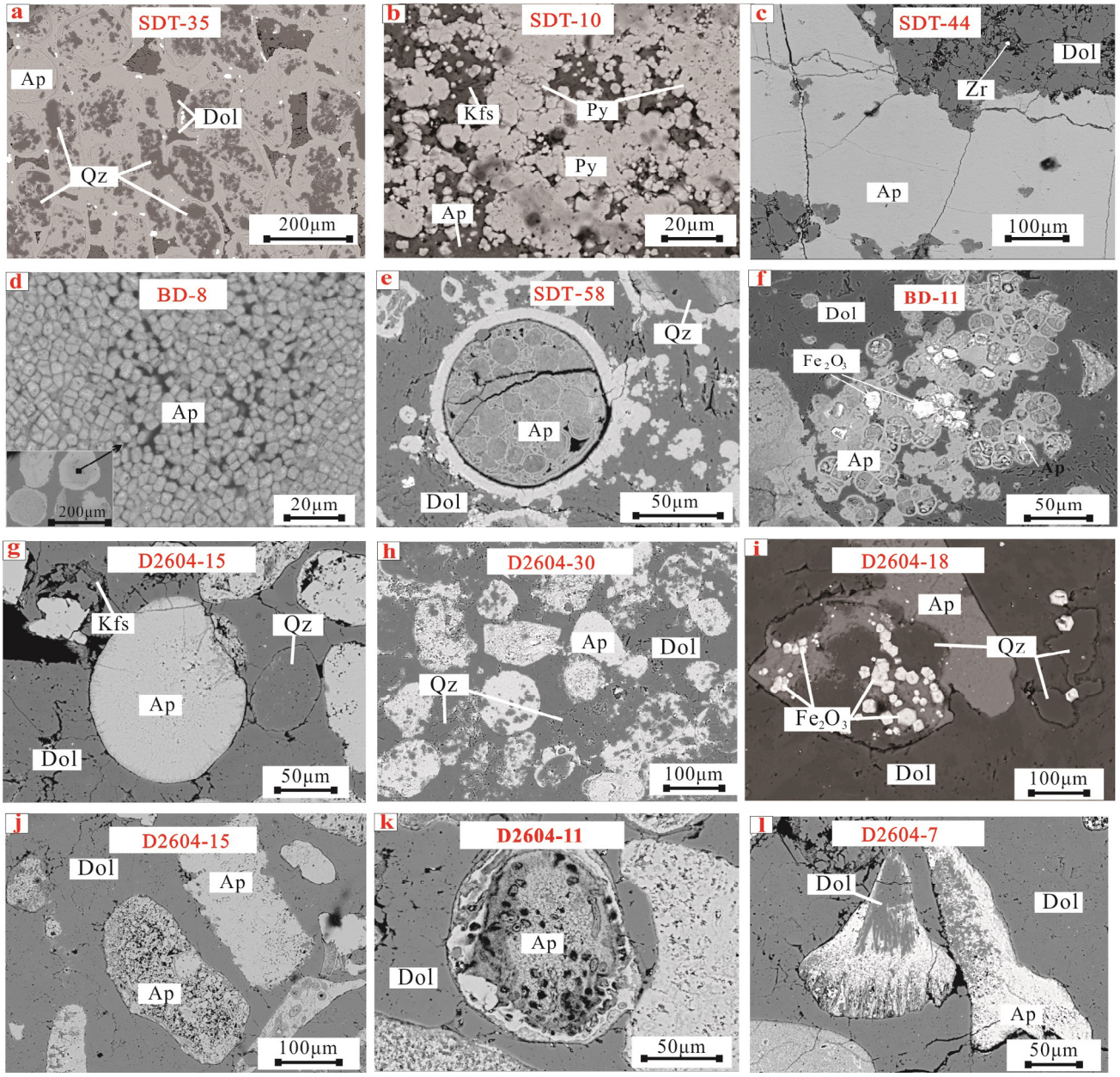

Fig. 6. Textural characteristics of the phosphate from Ediacaran and Cambrian in Weng'an and Zhijin, Central Guizhou. All these pictures were captured under backscattered electron. Abbreviations: SDT, samples from the Shangdatang profile in Weng'an; BD, samples from the Baidou profile in Weng'an; D, samples from the Motianchong drill hole in Zhijin; Dol = dolomite; Qtz = quartz; Ap = apatite; Kfs = K-feldspar; Zr = zircon.

Zhijin deposits (Fig. 4b, blue stars). The samples were fresh and sequential, including the ore-bearing formation, overlying strata, and underlying strata. All samples were analyzed to determine their petrographic characteristics, and the major and trace element compositions of most of samples were analyzed. The fresh and typical samples of Baidou profile and Shangdatang profile were chosen to be investigated the Mo, carbonate C and O, and phosphate O isotopic compositions. Detailed analytical methods are described below.

3.1. Major element analyses

The main elemental components of phosphorites and wall rocks were analyzed at the ALS Minerals (Guangzhou) Co Ltd, with X-ray fluorescence (XRF; ME-XRF24 for phosphorites, ME-XRF26 for wall rocks). Phosphorite samples were digested by $LiNO_3$ solution and wall rocks were digested by $Li_2B_4O_7$ and then melted at 1000 ℃. Another samples were burned at 1000 °C and subsequently weighted to obtain the loss on ignition (LOI). The sum of XRF analyses and LOIs was considered as the "sum total" with standard deviation less than 1%. The detection limit for all major oxides was 0.01 wt.% and the error was <3%.

3.2. Trace element analyses

Trace element analyses were conducted at the State Key Laboratory of Ore Deposit Geochemistry of the Institute of Geochemistry, Chinese Academy of Sciences in Guiyang, using a quadrupole inductively coupled plasma mass spectrometer (Q-ICP-MS), model ELAN-DRC-e ICP-MS (PerkinElmer, Inc., USA), with a relative standard deviation generally better than 10%. Portions (50 mg) of the samples were completely digested using a mixed

HF and HNO_3 solution. The analytical method was according to Qi et al. (2000), and the internal standard was a 40 ng/mL Rh solution. The detection limits were as follows: Tb, Ho, Lu, and Tm (0.01 ppm); Er, Eu, Sm, Pr, and Yb (0.03 ppm); Ce, Gd, and Dy (0.05 ppm); Hf (0.2 ppm); Nd (0.1 ppm); Y and La (0.5 ppm); Zr and Mo (2 ppm). The Eu/Eu*, Ce/Ce*, and Ce_{anom} were calculated according to following equations: $Eu/Eu^* = 2Eu_N/(Sm_N + Gd_N)$, $Ce/Ce^* = 2Ce_N/(La_N + Nd_N)$ (Bau and Dulski, 1996); $Ce_{anom} = lg(3 \times Ce_N/(2 \times La_N + Nd_N)$ (Haskin et al., 1968).

3.3. Petrographic analyses

The micro-textures of minerals were analyzed at the State Key Laboratory of Ore Deposit Geochemistry of the Institute of Geochemistry, Chinese Academy of Sciences. The samples were made into polished sections with 30-μm thickness, the petrographic characteristics were analyzed via a JSM-7800F field emission SEM (Jeol Ltd., Japan). The beam emitted by the electric gun was turned into a high-energy electric beam by a 10–30 kV acceleration voltage and then focused as a 1-μm microbeam to bombard the surface of the minerals. The secondary and backscattered electrons were detected and analyzed by the SEM. The backscattered electron images were collected with a 10-kV, 4.5-mA beam and secondary electron images were collected with a 20-kV, 4.5-mA beam.

3.4. Carbonate C and O isotopic analyses

The dolomite C and O isotopes were analyzed at the State Key Laboratory of Ore Deposit Geochemistry Institute of Geochemistry, Chinese Academy of Sciences. The phosphorite sample powder was collected on a weighing paper and then transferred to a standard 12-mL headspace sample vial or a 3-mL vial, depending on the sample size. The samples were then flushed with helium using a Gasbench II device (Thermo Fischer Scientific, USA) for 8 min. Phosphoric acid was manually dosed to the flushed samples to generate the analyte CO_2. The samples and acid were reacted at 72 °C for at least 4 h and then measured for $\delta^{13}C$ and $\delta^{18}O$ using a Gasbench II attached to the MAT253 gas source isotope ratio mass spectrometer. The (Vienna) Standard Mean Ocean Water (SMOW) and Pee Dee Belemnite (PDB) were used as the $\delta^{18}O$ and $\delta^{13}C$ standards, respectively. The conversion formula of $\delta^{18}O$ values is as follows: $\delta^{18}O_{SMOW}$ (‰) = 1.03091 × $\delta^{18}O_{PDB}$ + 30.91 (Coplen et al., 1983)

3.5. Phosphate O isotopic analyses

Phosphate O isotopic analyses were conducted at the Beijing Research Institute of Uranium Geology using a MAT253 isotope mass spectrometer. The selected apatites were dissolved using 1-mol/L HNO_3 for 8 h and then a BIO-RAD AG50-X8 cation exchange resin was poured in for positive ion scavenging. The liquid was vibrated for at least 8 h and then filtered. Excess $AgNO_3$ was added into the filter solution, making the PO_4^{3-} separate out entirely as Ag_3PO_4. Additionally, 300 μg of Ag_3PO_4 and a Ni-plated carbon rod reacted to produce CO at 1350 ℃ in a pyrolyzing furnace. The CO was measured for $\delta^{18}O$ by the MAT253 mass spectrometer using SMOW as the standard.

3.6. Mo isotopic analyses

The Mo isotopic composition of Doushantuo phosphorites from the Baidou profile was analyzed in this study, while that of Gezhongwu phosphorites was cited from Liu (2017). Both them were analyzed at the State Key Laboratory of Ore Deposit Geochemistry Institute of Geochemistry, Chinese Academy of Sciences using a Neptune Plus multi-receiver inductively coupled plasma mass spectrometer (MC-ICP-MS; Thermo Fisher Scientific, USA). Two grams of samples and 10 mL of HF were put into a polytef beaker and heated for 4 h; then, 20 mL of HNO_3 was added and heated for 12 h. This step allowed complete dissolution of the sample. We continued to add 3 mL $HClO_4$ to remove OM and then the $HClO_4$ was scavenged by 5 mL of HNO_3. This solution was made into a 6 mol/L HCL solution. An improved anion/cation exchange resin double-column procedure, using an AG50W-X8 cation exchange resin and AG1-X8 anion exchange resin, was adopted to separate the Mo from the concomitant elements (Zhang et al., 2009), ensuring that all traces of Mo in the resin were totally eluted. The Mo solution obtained was made into 200 ppb of HCl solution and Mo isotopic measurements were performed on a Neptune Plus MC-ICP-MS, with an analytical precision of 0.05‰.

Molybdenum isotopic ratios have been reported using the delta notation for two ratios, $^{98/95}Mo$ and the $d^{97/95}Mo$, which may be calculated by the following formula: $\delta^{98/95}Mo = (^{98/95}Mo_{sample} - ^{98/95}Mo_{standard}) / ^{98/95}Mo_{standard} \times 1000$ (Nägler et al., 2014) and $\delta^{97/95}Mo = 2/3 \times \delta^{98/95}Mo$. Even though a universally accepted international measurement standard is lacking, NIST SRM 3141 is often used as the Mo isotope standard, and the $\delta^{98/95}Mo$ of the NIST SRM 3134 is 0.25‰ (Nägler et al., 2014).

4. Analytical results

4.1. Major element contents

The major element composition of Doushantuo and Gezhongwu phosphorite, including P_2O_5, F, CaO, MgO, SiO_2, Al_2O_3, and TFe_2O_3, is detailed in Table 1 and Supplementary data Table S1. The mean values of P_2O_5, F, CaO, MgO, and SiO_2 contents of the Lower Doushantuo were 30.36 wt.%, 2.93 wt.%, 44.08 wt.%, 1.57 wt.%, and 11.38 wt.%, respectively, while those of the Upper Doushantuo Formation were 20.40 wt.%, 2.16 wt.%, 42.23 wt.%, 10.05 wt.%, and 2.11 wt.%, respectively. The content of SO_2 and total Fe (TFe_2O_3) for Lower Doushantuo were much higher (0.33–3.47, 0.44–1.36, respectively) than that of Upper Doushantuo (0.02–0.56, 0.10–0.93, respectively). The mean values P_2O_5, F, CaO, MgO, TFe_2O_3, SO_3, and SiO_2 contents of the Lower Gezhongwu were 17.86 wt. %, 1.82 wt.%, 40.72 wt.%, 10.84 wt.%, 0.96 wt.%, 0.14 wt.%, and 2.05 wt.%, respectively, while those of the Upper Gezhongwu Formation were 6.25 wt,%, 0.74 wt,%, 29.55 wt,%, 14.13 wt,%, 1.40 wt,%, 0.76 wt.%, and 13.60 wt.%, respectively. The P_2O_5 content of Doushantuo phosphorites was much higher than that of Gezhongwu samples, and the Doushantuo deposits are middle–high grade whereas the Gezhongwu phosphorites are middle–low grade.

4.2. Zr/Hf ratios

The Zr and Hf composition of Doushantuo and Gezhongwu phosphorites are detailed in Tables 2 and 3, respectively. The Zr/Hf ratios in the Lower Doushantuo exhibited little variation ranging from 45.00 to 70.00 (mean: 57.26) while that of the Upper Doushantuo displayed substantial variation ranging from 4.50 to 60.00 (mean: 28.52). Generally, the Upper Doushantuo have lower Zr/Hf than that of Lower Doushantuo, and the mean Zr/Hf value of interbedded dolomite was 34.00. The Zr/Hf ratios in the Lower and Upper Gezhongwu Formation range from 15.62 to 36.22 (mean: 21.53) and 17.67 to 35.30 (mean: 26.73), respectively, showing a lower mean value than the Doushantuo Formation. Even though the Upper Doushantuo show largest variance with a standard deviation of 17.67, Zr/Hf values decreased from the bottom of the Doushantuo Formation to the top of Gezhongwu Formation.

Table 1
Major element concentrations (in wt.%) of the Gezhongwu Formation from the Motianchong drill hole, Zhijin.

Stratum	Sample	Al_2O_3	CaO	F	TFe_2O_3	K_2O	MgO	P_2O_5	SiO_2	SO_3	LOI	Sum
Niutitang Fm.	D26-40	2.83	26.6	–	4.09	0.45	11.70	1.43	15.86	7.32	30.15	100.43
Upper Gezhongwu (ϵ_1gz^2)	D26-39	0.66	28.5	0.9	0.67	0.22	12.30	8.27	21.20	0.05	27.35	100.12
	D26-37	1.61	32.6	1.2	2.03	0.53	10.90	11.45	13.05	0.63	25.87	99.87
	D26-33	0.75	27.8	0.3	1.00	0.24	16.85	3.05	12.40	0.03	37.43	99.85
	D26-30	1.18	27.6	0.5	0.66	0.37	15.85	3.84	15.35	0.04	34.91	100.30
	D26-28	0.87	28.2	0.4	0.98	0.28	17.25	2.92	10.55	0.04	38.30	99.79
	D26-25	0.22	41.5	1.9	0.65	0.08	10.90	18.55	1.22	0.09	25.25	100.36
	D26-23	0.97	28.5	0.4	0.93	0.31	16.80	3.53	10.85	0.03	37.39	99.71
	D26-22	1.58	28.9	1.0	1.71	0.52	11.80	8.94	18.55	0.06	26.66	99.72
	D26-21	0.73	27.0	0.5	1.39	0.24	14.75	4.15	17.55	0.03	33.48	99.82
	D26-19	0.46	27.8	0.3	1.30	0.15	16.30	2.65	13.05	0.04	37.63	99.68
	Median	**0.81**	**28.20**	**0.50**	**1.00**	**0.28**	**14.75**	**3.84**	**13.05**	**0.04**	**33.48**	**99.85**
n = 10	**Mean**	**1.08**	**29.55**	**0.74**	**1.40**	**0.31**	**14.13**	**6.25**	**13.60**	**0.76**	**32.22**	**0.25**
	δ	**0.45**	**4.37**	**0.51**	**0.47**	**0.15**	**2.61**	**5.16**	**5.50**	**0.19**	**5.50**	**5.50**
Lower Gezhongwu (ϵ_1gz^1)	D26-17	0.37	32.5	0.5	2.17	0.12	17.45	4.71	2.14	0.04	40.21	100.21
	D26-15	0.23	36.5	1.2	1.31	0.08	14.35	11.05	1.85	0.06	33.41	100.04
	D26-13	0.24	39.2	1.5	0.79	0.09	12.10	15.50	2.24	0.08	28.16	99.90
	D26-11	0.30	35.2	1.0	1.25	0.08	15.20	9.32	3.10	0.06	34.79	100.30
	D26-10	0.21	38.0	1.4	0.81	0.08	13.10	13.65	1.72	0.07	30.49	99.53
	D26-7	0.32	50.5	3.3	0.63	0.11	2.91	33.2	1.26	0.17	7.94	100.34
	D26-5	0.24	49.5	3.1	0.65	0.08	4.21	31.0	0.84	0.18	10.78	100.58
	D26-3	0.78	45.5	2.7	0.43	0.28	6.70	25.7	1.80	0.25	15.84	99.98
	D26-2	0.59	39.6	1.7	0.64	0.20	11.50	16.60	3.49	0.36	25.90	100.58
	Median	**0.30**	**39.20**	**1.50**	**0.79**	**0.09**	**12.10**	**15.50**	**1.85**	**0.08**	**28.16**	**100.21**
n = 9	**Mean**	**0.36**	**40.72**	**1.82**	**0.96**	**0.12**	**10.84**	**17.86**	**2.05**	**0.14**	**25.28**	**100.16**
	δ	**0.19**	**6.35**	**0.98**	**0.54**	**0.07**	**5.08**	**9.92**	**0.83**	**0.11**	**11.27**	**0.34**
Dengying Fm.	D26-1	0.27	32.6	–	0.35	0.10	18.70	2.28	1.56	0.09	43.47	99.42

Fig. 7 show the decreasing trend of Zr/Hf. In order to compare with the C and O isotope, the Zr/Hf was from Baidou profile according to Yang et al. (2019).

4.3. REE characteristics

The REEs of the Doushantuo and Gezhongwu phosphorites are listed in Supplementary data, Table S2. Here, the contents of REY (∑REY) display a relatively broad range from 28.10 ppm to 346.93 ppm, with a mean value of 218.24 ppm in the Lower Doushantuo and 85.49 ppm in the Upper Doushantuo. The ∑REY of cap and interlayer dolomite is low, and that of Dengying Formation was 49.71 ppm. The ∑REY of Gezhongwu phosphorites is much higher than that of Doushantuo phosphorites. Moreover, the ∑REY of Gezhongwu phosphorites exhibits a large range of variation from 123.92 ppm to 1113.87 ppm, with a mean of 708.60 ppm in the Lower Gezhongwu and a mean of 375.73 ppm in the Upper Gezhongwu. The mean ∑REY for the Dengying dolomite and Niutitang sandy shale are 59.52 ppm and 86.95 ppm, respectively. In Doushantuo phosphorite, ∑REY is weakly and positively correlated with P_2O_5, while in Gezhongwu phosphorite, ∑REY shows markedly positive correlations with P_2O_5 (Fig. 8a).

The Y/Ho ratios of the Lower Doushantuo range from 36.00 to 45.75, with a mean of 42.40, which is slightly higher than those of the Upper Doushantuo (36.18–46.25, mean: 40.22). The Y/Ho ratios of the Lower Gezhongwu range from 15.95 to 48.17, with a mean of 35.98, which is lower than those of the Upper Gezhongwu (40.31–52.77, mean: 45.23). Moreover, Y/Ho is negatively correlated with ∑REY, except in the Upper Doushantuo (Fig. 8b).

The cerium anomaly (Ce_{anom}) and Eu/Eu* of the Lower Doushantuo are −0.12 to −0.06 (mean: −0.08) and 0.93 to 1.01 (mean: 0.98), respectively, while the Ce_{anom} and Eu/Eu* of the Upper Doushantuo are −0.41 to −0.17 (mean: −0.28) and 0.83 to 1.05 (mean: 0.94), respectively. The Ce_{anom} and Eu/Eu* of the Lower Gezhongwu are 0.53 to −0.41 (mean: −0.49) and 0.91 to 1.24 (mean: 0.99), and those of the Upper Gezhongwu are −0.52 to −0.40 (mean: −0.45) and 0.90–1.15 (mean: 1.02). The Ce_{anom} display a negative shift immediately at the bottom of the Upper Doushantuo, with negative values persisting until the Gezhongwu Formation. The Ce_{anom} and ∑REY are negatively correlated when $Ce_{anom} < -0.1$, and no correlation is observed when $Ce_{anom} > -0.1$ in the Doushantuo phosphorites. In all Gezhongwu phosphorite samples, Ce_{anom} is not correlated with ∑REY (Fig. 8c).

The PAAS-normalized REY distributions of the Lower Doushantuo are characterized by the pronounced enrichment of heavy REEs (HREEs) in comparison with light REEs (LREEs), belonging to "seawater-like" type (Fig. 9a). Meanwhile, those of the Upper Doushantuo show "hat-shaped" REY plots, characterized by the enrichment of middle REEs (MREEs) in comparison with those of LREEs and HREEs (Fig. 9a). La_N/Gd_N ratios range from 0.34 to 0.51 and Gd_N/Yb_N ratios range from 0.89 to 1.44 for Lower Doushantuo phosphorite; while those of Upper Doushantuo phosphorite were 0.20–0.55 and 1.32–2.77, respectively. The wall rocks of the Doushantuo Formation show flat REY plots (Fig. 9b). For the Gezhongwu phosphorites, both the Lower and Upper Gezhongwu show "hat-shaped" PAAS-normalized REY distributions (Fig. 9c), while the country rocks show flat REY plots with inconspicuous MREE enrichment (Fig. 9d). La_N/Gd_N and Gd_N/Yb_N ratios ratios of Lower Gezhongwu were 0.40–0.82, 1.31–2.63, and those of Upper Gezhongwu were 0.28–0.80, 1.18–2.68, respectively.

The variation tendency of P_2O_5, REY, and Y/Ho from Ediacaran to Early Cambrian are shown in Fig. 7. The P_2O_5 of the Doushantuo Formation was much higher than that of the Gezhongwu, while the ∑REY was greater in the Gezhongwu Formation. Additionally, ∑REY tended to vary consistently with P_2O_5 but oppositely with Y/Ho, which is consistent with the correlations (Fig. 8). Furthermore, REY and Y/Ho ratios were relatively stable in the Doushantuo Formation while exhibited pulsed variation in the Gezhongwu Formation, especially in the Lower Gezhongwu.

4.4. Carbonate C and O isotopes

The C and O isotopic concentrations of Gezhongwu and Doushantuo carbonates are listed in Table 4. The Lower Doushantuo display negative $\delta^{13}C_{PDB}$ values ranging from − 3.30‰ to − 2.41‰, and a narrow range of $\delta^{18}O_{SMOW}$ from 21.27‰ to 23.11‰.

Table 2
Zirconium and hafnium of the Doushantuo Formation from the Weng'an Shangdatang profile.

Stratum	Sample No.	Zr (ppm)	Hf (ppm)	Zr/Hf	Stratum	Sample No.	Zr (ppm)	Hf (ppm)	Zr/Hf	Stratum	Sample No.	Zr (ppm)	Hf (ppm)	Zr/Hf
Dengying Fm.	SDT-68	6.40	0.20	32.00	Upper Doushantuo	SDT-43	3.00	0.20	15.00	Lower Doushantuo	SDT-23	56.00	1.10	50.91
Upper Doushantuo	SDT-67	<0.5	0.20	25.00		SDT-42	12.00	0.30	40.00		SDT-22	39.00	0.60	65.00
	SDT-66	<0.5	0.20	23.50		SDT-41	9.10	0.20	45.50		SDT-21	44.00	0.90	48.89
	SDT-65	1.80	0.20	9.00		SDT-40	9.20	0.20	46.00		SDT-20	40.00	0.70	57.14
	SDT-64	12.00	0.20	44.50		SDT-39	8.30	0.20	41.50		SDT-19	44.00	0.80	55.00
	SDT-63	12.00	0.30	40.00	**n = 26**	**Median**	**6.35**	**0.2**	**29.5**		SDT-18	46.00	0.70	65.71
	SDT-62	6.50	0.20	32.50		**Mean**	**7.06**	**0.23**	**28.52**		SDT-17	50.00	0.90	55.56
	SDT-61	12.00	0.20	60.00		**δ**	**5.36**	**0.07**	**17.67**		SDT-16	27.00	0.60	45.00
	SDT-60	6.20	0.20	31.00	Interlayer dolomite	SDT-38	4.00	0.20	20.00		SDT-15	37.00	0.70	52.86
	SDT-59	11.00	0.20	55.00		SDT-37	6.40	0.20	32.00		SDT-14	36.00	0.70	51.43
	SDT-58	19.00	0.50	38.00		SDT-36	15.00	0.30	50.00		SDT-13	35.00	0.50	70.00
	SDT-57	2.90	0.20	14.50	Lower Doushantuo	SDT-35	31.00	0.50	62.00		SDT-12	33.00	0.50	66.00
	SDT-56	5.60	0.20	28.00		SDT-33	72.00	1.50	48.00		SDT-11	32.00	0.50	64.00
	SDT-53	0.90	0.20	4.50		SDT-32	50.00	0.90	55.56		SDT-10	34.00	0.60	56.67
	SDT-52	1.60	0.20	8.00		SDT-31	60.00	1.10	54.55		SDT-9	34.00	0.50	68.00
	SDT-51	2.00	0.20	10.00		SDT-30	50.00	0.80	62.50		SDT-8	33.00	0.60	55.00
	SDT-50	1.20	0.20	6.00		SDT-29	55.00	0.90	61.11		SDT-7	34.00	0.60	56.67
	SDT-49	2.30	0.20	11.50		SDT-28	65.00	1.40	46.43	**n = 28**	**Median**	**44.36**	**0.79**	**57.26**
	SDT-48	0.90	0.20	4.50		SDT-27	52.00	0.90	57.78		**Mean**	**44.36**	**0.79**	**57.26**
	SDT-47	1.60	0.20	8.00		SDT-26	51.00	0.80	63.75		**δ**	**11.29**	**0.26**	**6.72**
	SDT-45	14.00	0.30	46.67		SDT-25	51.00	1.00	51.00	cap dolomite	SDT-6	5.30	0.20	26.50
	SDT-44	15.00	0.30	50.00		SDT-24	51.00	0.90	56.67		SDT-2	8.50	0.20	42.50

The Upper Doushantuo exhibit $\delta^{13}C_{PDB}$ values ranging from − 4.3‰ to 1.11‰, and a wide range of $\delta^{18}O_{SMOW}$ from 19.73‰ to 29.33‰. A positive $\delta^{13}C_{PDB}$ excursion is observed at the lower part of the Upper Doushantuo and lasts until the Gezhongwu. There is a narrow $\delta^{13}C_{PDB}$ range near 0‰ in both the Lower (−0.58‰ to 0.49‰) and Upper (−2.79‰ to − 0.04‰) Gezhongwu formations. The $\delta^{18}O_{SMOW}$ of the Lower Gezhongwu (18.69‰ to 20.31‰) is lower than that of the Upper Gezhongwu (22.66‰ to 25.86‰).

The variations of $\delta^{13}C_{PDB}$ and $\delta^{18}O_{SMOW}$ from Doushantuo to Gezhongwu times are shown in Fig. 7. The $\delta^{13}C_{PDB}$ and $\delta^{18}O_{SMOW}$ exhibite consistent variation in the Doushantuo Formation, while the opposite is true in the Gezhongwu Formation (Fig. 10a). The correlations suggest the presence of a negative relationship between ∑REY and $\delta^{13}C_{PDB}$ in Doushantuo carbonates and a positive relationship in Gezhongwu carbonates (Fig. 10b). The ∑REY are positively correlated with $\delta^{18}O_{SMOW}$ in both Doushantuo and Gezhongwu carbonates (Fig. 10c).

4.5. Phosphate O isotopes

The phosphate O isotopic compositions are shown in Table 5, with SMOW used as the standard. The data suggest that the $\delta^{18}O_p$ of the Lower Doushantuo lies within a narrow range (17.4%–17.9‰) and that $\delta^{18}O_p$ decreases gradually in the Upper Doushantuo, falling to 15.0‰ at the top of the formation. The $\delta^{18}O_p$ in the Gezhongwu Formation is variable ranging from 14.6% to 19.5‰ (mean: 17.31‰) in the Lower Gezhongwu and from 11.10% to 17.00‰ in the Upper Gezhongwu (mean: 15.11‰), showing a decreasing trend (Fig. 11).

The fractionation values between dolomite and phosphate ($\Delta^{18}O_{CO_3\text{-}PO_4}$) indicate the isotope fractionation degree. In our samples, $\Delta^{18}O_{CO_3\text{-}PO_4}$ of Lower Doushantuo were 3.78–5.22, while those of Upper Doushantuo reached up to 10.50–11.84. The Gehzongwu phosphorite and dolomite had variable $\Delta^{18}O_{CO_3\text{-}PO_4}$ ranging of 0.12–14.77, with higher fractionation values in the Upper Gezhongwu than those of Lower Gezhongwu.

4.6. Mo isotopes

Terrigenous detrital materials may influence the Mo contents of phosphorite deposits because of the low proportion of Mo in phosphorites/carbonates. Here, detrital Mo was calculated as follows (Rudnick and Gao, 2003): $Mo_{detrital} = [(Mo/X)_{upper\ crust}] \times X_{Sample}$, wherein X represents Al or Ti. The Al_2O_3 and Mo contents were 15.2% and 1.5 ppm, respectively according to Institute of Geochemistry (1998). We used Mo_{EF} to represent the Mo content of seawater: $Mo_{EF} = Mo_{sample} - Mo_{detrital}$. The results revealed a negligible Mo contribution from terrigenous detrital materials (Table 6). The Mo contents exhibited a narrow range in the Lower Doushantuo (0.19–0.21 ppm) but a wide range in the Upper Doushantuo (0.03–1.09 ppm). Meanwhile, those in the Gezhongwu phosphorites, according to Liu (2017), are generally much higher than in Doushantuo phosphorites. Moreover, the Upper Gezhongwu has a higher Mo content (3.73–40.00 ppm, mean: 12.78 ppm) than the Lower Gezhongwu (0.19–1.49 ppm, mean: 0.72 ppm).

The Mo isotopic compositions show that phosphorites from the Lower Doushantuo yield $\delta^{98/95}$Mo values of 0.70‰ ± 0.03‰ and 1.34‰ ± 0.04‰, while those of the Upper Doushantuo have a wider range (−1.13‰ to 0.80‰). A positive excursion occurs at the top of the Lower Doushantuo (1.34‰) and a negative excursion occurs at the top of the Upper Doushantuo (−1.13‰). The measured $\delta^{98/95}$Mo values generally decrease from the bottom to the top of the Doushantuo Formation. The $\delta^{98/95}$Mo values of Gezhongwu phosphorites are generally heavier than those of Doushantuo phosphorites, wherein the $\delta^{98/95}$Mo of the Lower Gezhongwu range

Table 3
Zirconium and hafnium of the Gezhongwu Formation from the Motianchong drill hole, Zhijin.

Stratum	Sample No.	Zr (ppm)	Hf (ppm)	Zr/Hf	Stratum	Sample No.	Zr (ppm)	Hf (ppm)	Zr/Hf
Niutitang Fm.	D26-41	228.77	5.67	40.37	**n = 21**	**Mean**	**15.18**	**0.60**	**26.73**
	D26-40	29.54	0.67	44.28		**δ**	**11.92**	**0.45**	**5.29**
Upper Gezhongwu	D26-39	10.59	0.47	22.55	Lower Gezhongwu	D26-18	13.04	0.57	22.69
	D26-38	14.95	0.47	31.79		D26-17	5.85	0.29	20.25
	D26-37	24.11	0.84	28.78		D26-16	14.93	0.63	23.86
	D26-36	15.93	0.63	25.28		D26-15	8.94	0.25	36.22
	D26-35	8.42	0.26	32.55		D26-14	17.79	1.02	17.41
	D26-34	11.30	0.38	30.01		D26-13	9.96	0.61	16.45
	D26-33	7.82	0.22	35.30		D26-12	15.84	0.80	19.83
	D26-32	13.44	0.47	28.50		D26-11	6.86	0.44	15.62
	D26-31	7.96	0.41	19.32		D26-10	7.48	0.37	20.11
	D26-30	10.65	0.44	24.14		D26-9	18.69	1.07	17.48
	D26-29	10.56	0.56	18.97		D26-8	5.53	0.30	18.29
	D26-28	8.08	0.25	31.89		D26-7	15.51	0.89	17.37
	D26-27	13.67	0.61	22.34		D26-6	10.34	0.39	26.36
	D26-26	11.19	0.38	29.28		D26-5	16.36	0.72	22.72
	D26-25	12.42	0.61	20.35		D26-4	11.99	0.51	23.74
	D26-24	40.98	1.46	28.00		D26-3	20.78	0.80	26.01
	D26-23	8.53	0.28	30.04		D26-2	11.00	0.35	31.71
	D26-22	21.66	0.81	26.88	**n = 17**	**Median**	**11.99**	**0.57**	**20.25**
	D26-21	10.63	0.31	34.82		**Mean**	**12.49**	**0.57**	**21.53**
	D26-20	49.14	2.14	22.95		**δ**	**4.69**	**0.26**	**5.58**
	D26-19	6.78	0.38	17.67	Dengying Fm.	D26-1	5.29	0.17	30.37
	Median	**11.25**	**0.47**	**28.25**					

from 1.13‰ to 1.80‰, and that of Upper Gezhongwu range from 1.98‰ to 2.39‰ with multiple isotopic variations.

5. Discussion

5.1. Sources of ore-forming materials

5.1.1. Potential sources of P

The atomic exchange of O in marine systems occurring among seawater, authigenic apatite, and dissolved phosphate (Chen et al., 2010) is controlled by microbial metabolism and temperature (Longinelli and Nuti, 1973; Blake et al., 1997). Researches showed that P-O bond was stable under ambient conditions in the ocean, and only by enzymatic catalysis the P-O bond was broken and oxygen isotope composition altered, which is a thermodynamic fractionation (Kolodny et al., 1983; Blake et al., 2005; Angert et al., 2012). When the microbio participated in the phosphate formation, the oxygen isotope fractionated between water and authigenic apatite, and the isotopic fractionation may equilibrate with ocean temperature (Longinelli and Nuti, 1973; Kolodny et al., 1983; Blake et al., 1997, 2005; Paytan et al., 2002). Longinelli and Nuti (1973) established the equilibrium equation for the first time according to the $\delta^{18}O_p$ and $\delta^{18}O_{water}$ of marine organisms lived in different temperatures: T(℃) = 111.4–4.3($\delta^{18}O_p$–$\delta^{18}O_{water}$). Which was then proved to be justified in Archean phosphate rocks (Blake et al., 2010), modern ocean (Colman et al., 2005; Goldhammer et al., 2011a), and laboratory experimental data (Blake et al., 2005).

The most important precondition for O isotope tracers of P is the significant difference among different origins. However, equilibrium fractionation would mask the original O isotope information (Blake et al., 2005; Colman et al., 2005). Longinelli et al. (1976) shows that the oxygen isotope composition of dissolved phosphate is not in equilibrium with sea water at any reasonable temperature, and non-equilibrated fractionation took place in aquatic environments, marine-sediment ecosystems (Blake et al., 2005; Colman et al., 2005; Goldhammer et al., 2011a). This might be attributed to the release of inorganic phosphorus with lighter oxygen isotope during the hydrolysis of organophosphorus (Blake et al., 2005; Colman et al., 2005; Goldhammer et al., 2011a). After Marinoan glaciers, the global climate warmed and weathering increased, resulting in upwelling to prevail and make South China an open marine system (Ye, 1989; Mi, 2010). Therefore, the O isotopes would not have reached equilibrium fractionation with abundant nutrient supply. Hence, we speculate that the original phosphate O isotope information were recorded in phosphorite, and the $\delta^{18}O_p$ values of phosphorites could reflect the $\delta^{18}O_p$ compositions of source-rocks only if useful depositional signals were excluded.

Precipitated P may undergo diagenetic transformations, including regeneration of inorganic phosphate, recrystallization, redistribution among different sedimentary P phases (Ruttenberg and Berner, 1993; Lecuyer et al., 1999; Jaisi and Blake, 2010; Goldhammer et al., 2011a), and supergene diagenesis (McArthur and Herczeg, 1990; Lecuyer et al., 1999). The dissolution and recrystallization resulted the isotope redistribution in mineral phases (Jaisi et al., 2011). Past years' studies showed that oxygen isotopes fractionation between carbonate and phosphate ($\Delta^{18}O_{CO_3\text{-}PO_4}$) tend to decrease with age and approach 0‰ for some old phosphorite samples (McArthur and Herczeg, 1990; Lecuyer et al., 1999). Here we compared the oxygen isotopic compositions of dolomite and phosphate, $\Delta^{18}O_{CO_3\text{-}PO_4}$ in our samples had greater variation, not related to burial time. Most of the samples from Upper Doushantuo and Upper Gezhongwu had close $\Delta^{18}O_{CO_3\text{-}PO4}$ values with recent phosphorites (~8‰) (Shemesh et al., 1988; McArthur and Herczeg, 1990), indicating limited diagenetic redistribution of oxygen isotope and the initial isotopic composition recorded by phosphate. Furthermore, the phosphate were deemed a more reliable proxy recording the initial isotopic signals than other oxyanions, such as carbonates, and sulfides (Fortier and Luttge, 1995; Zazzo et al., 2004). Hence, $\delta^{18}O_p$ value have proven to be useful indicators to reflect source contributions or biological recycling (Blake et al., 2005; Colman et al., 2005; Young et al., 2009).

Due to the lack of $\delta^{18}O_p$ values in Ediacaran and Cambrian rocks and seawater, the studied $\delta^{18}O_p$ values of phosphorites were compared with the reported Archean and modern $\delta^{18}O_p$ data (Fig. 11). The authigenic phosphates can represent the seawater end-member (heavy end-member), while the igneous rocks and detrital

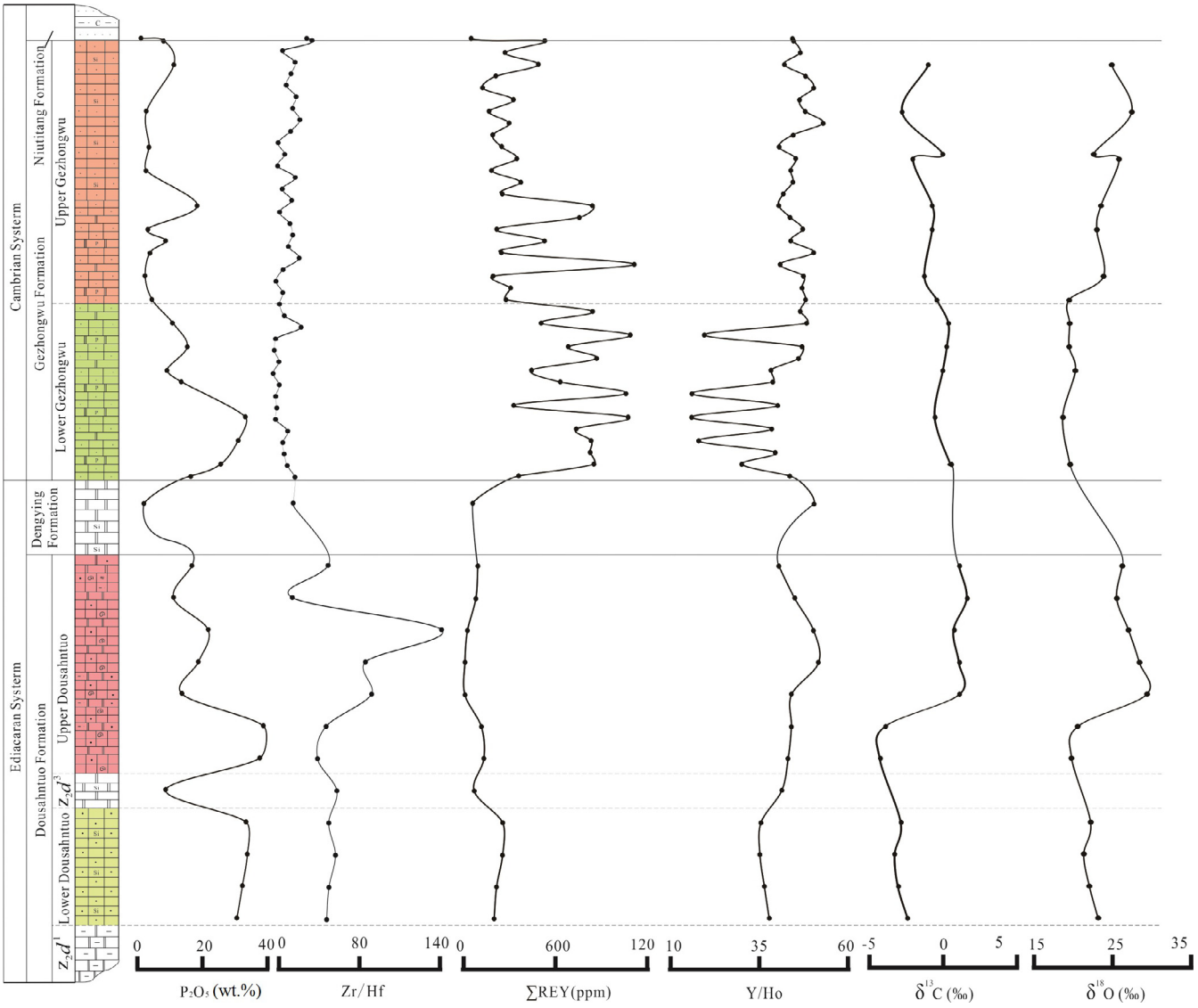

Fig. 7. Variation of REY, Zr/Hf, P_2O_5, Y/Ho, $\delta^{13}C_{VPDB}$, and $\delta^{18}O_{SMOW}$ from the Ediacaran to the Cambrian ages in Central Guizhou. Abbreviations: PDB = Pee Dee Belemnite; SMOW = (Vienna) Standard Mean Ocean Water.

apatite represent the terrigenous end-member (light end-member) (Yuan et al., 2019). The $\delta^{18}O_p$ values of phosphorites in this study ranged between those of authigenic phosphates and igneous rocks and detrital apatite (Fig. 11), reflecting the mixing of the two end-members. Liang and Blake (2007) conducted synthesis experiments in abiotic inorganic systerms, in which the $CaCO_3$ was added into mixed solution of KH_2PO_4 and NaF under 20−45℃ in order to yield apatite. Results showed that the fractionation value of solid- and aqueous-phosphate phase is approximately 1‰, which was consistent with other experimental results (−2‰ to 1‰, and 1‰, respectively) (Blake et al., 1997; Paytan et al., 2002). These results indicated that the apatites were 1‰-1.4‰ heavier than the initially added dissolved phosphate group. Thus, the original $\delta^{18}O_p$ might be lighter than that recorded by apatites and rather incline to detrital or igneous apatite than to seawater. Moreover, the $\delta^{18}O_p$ values showed a decreasing trend from the Lower Doushantuo to the Upper Gezhongwu, indicating that terrigenous weathering brought increased P, while the seawater performed inversely. According to the petrologic characteristics, the phosphorite from Upper Dousahntuo and Gezhongwu Formation were mainly composed of microbial debris (Fig. 6j–l). The $\delta^{18}O_p$ values in the Gezhongwu Formation have a wider range than those of the Doushantuo Formation, especially the Lower Doushantuo. It should be attributed to the microbial metabolism and oxygen isotope redistribution in the organic and inorganic P phrase in Cambrian phosphorite (Colman et al., 2005; Jaisi et al., 2011).

5.1.2. P sources and geochemical background

At PC/C boundary, a series of geodynamic changes occurred, including the Neoproterozoic Oxygenation Event (Och and Shields-Zhou, 2012), supercontinental break up (Veevers, 2004), Marinoan glacier melting (Walter et al., 2000), continental denudation (Reinhard et al., 2017), resulting in expanded terrestrial weathering and increased upwelling into shallow marine settings (Liu and Cao, 1987; Ye, 1989; Jiang et al., 2007; Föllmi et al., 2009; Mi, 2010; Planavsky et al., 2010). Consequently, margins that were favorably positioned for upwelling, such as Central Guizhou of South China during the PC/C, were bathed with upwelled deep seawater that was incredibly rich in P. The stratigraphic sequences of Doushantuo phosphorite in Hubei suggest that high-grade phosphorites correspond to periods of transgression (Mi, 2010), while the lithofacies paleogeography of Cambrian phosphorite along the western margin

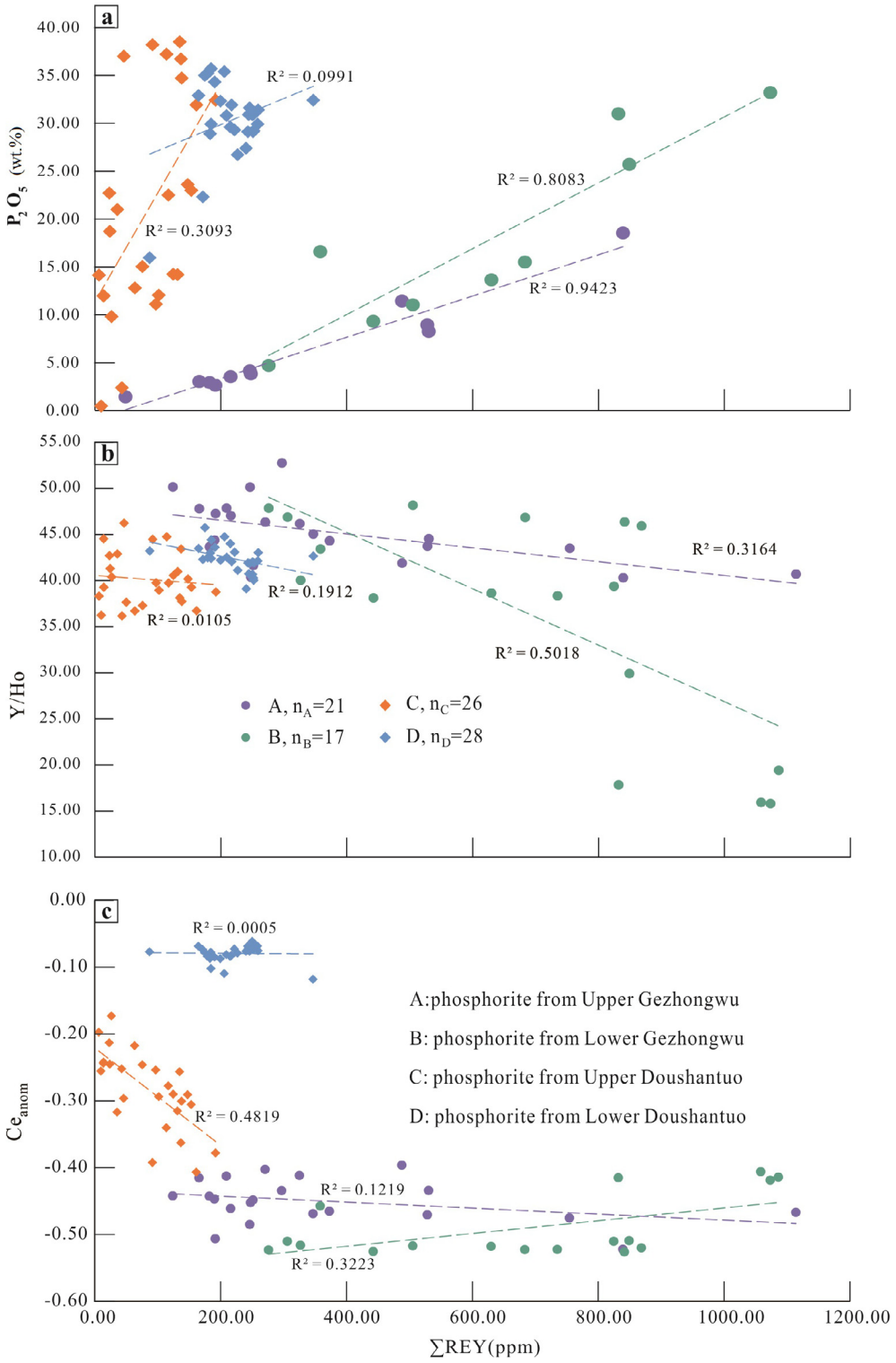

Fig. 8. Relationships between (a) ∑REY and P_2O_5, (b) ∑REY and Y/Ho, and (c) ∑REY and Ce_{anom}in the Ediacaran to early Cambrian phosphorites from Central Guizhou.

of the Yangtze Platform recorded storm activities (Liu et al., 1987), indicating that the ore-forming materials were brought along with upwelling currents and/or storm activities. Additionally, $\delta^{13}C$ values show the presence of ^{13}C-depleted deep-water carbonates and a strong surface-to-deep ocean $\delta^{13}C_{carb}$ gradient in the Ediacaran ocean (Jiang et al., 2007), which is indicative of a deep seawater origin (Kaufman and Knoll, 1995; Mi, 2010).

(Bio)chemical weathering on continents represents a significant source of bioavailable P (Föllmi, 1996; Filippelli, 2008; Pufahl and Groat, 2017). Oxygenated and warm conditions are beneficial to accelerate the hydrologic cycle, intensify chemical weathering, and amplify the flux of P to the ocean (Filippelli and Delaney, 1992; Föllmi, 1996; Filippelli, 2008). Another beneficial factor was widespread orogeny associated with amalgamation of

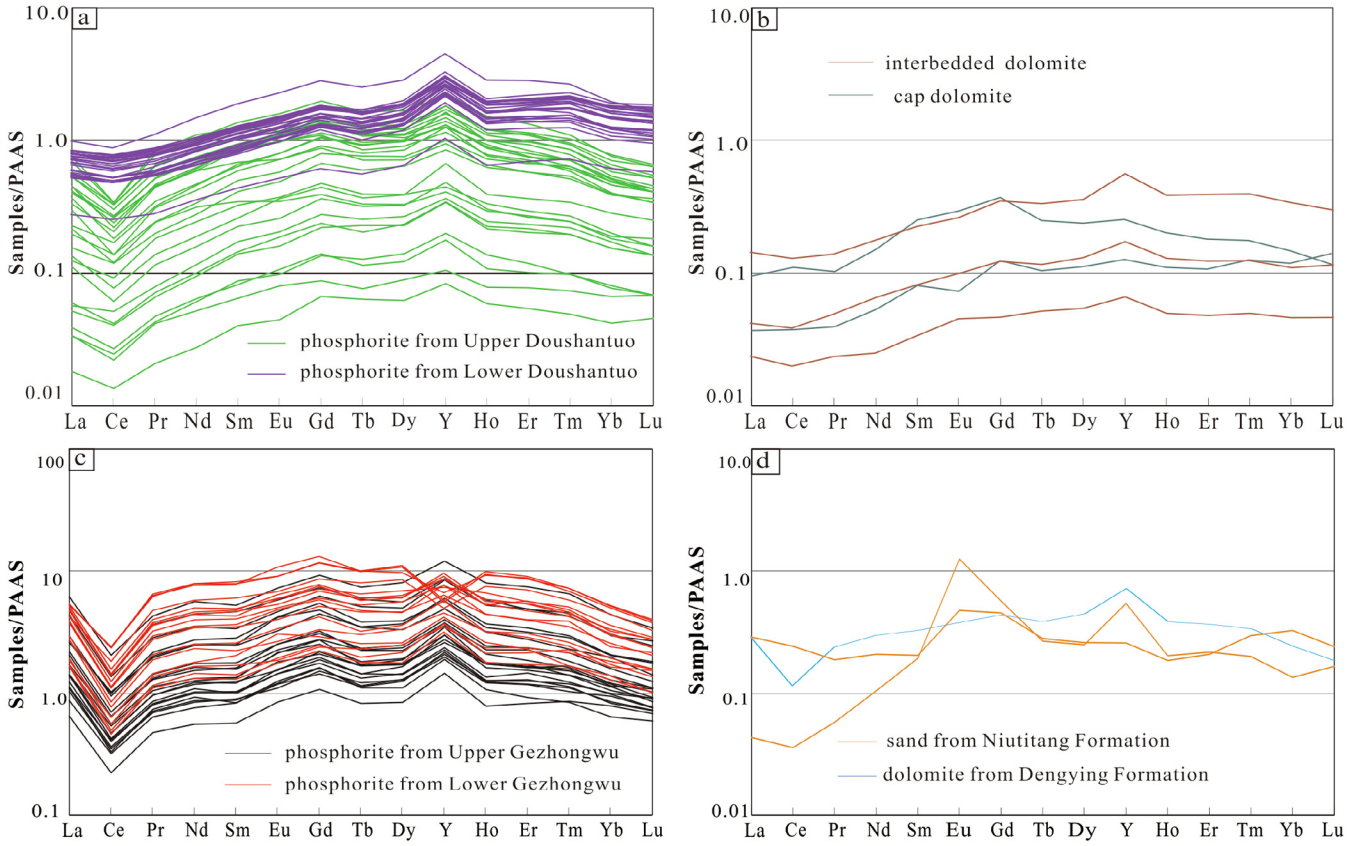

Fig. 9. The PAAS-normalized REY distributions of phosphorites (a) and wall rocks (b) from Weng'an deposit; The PAAS-normalized REY distributions of phosphorites (c) and wall rocks (d) from Zhijin deposit (PAAS data from Taylor and Mclennan, 1985).

Table 4
The REE concentrations and C and O isotopes of Doushantuo and Gezhongwu carbonates from Central Guihzou.

Stratum	Sample No.	∑REY (ppm)	P_2O_5 (wt.%)	$\delta^{13}C_{dol\text{-}VPDB}$ (‰)	Std.dev	$\delta^{18}O_{dol\text{-}VPDB}$ (‰)	$\delta^{18}O_{dol\text{-}SMOW}$ (‰)	2δ
	D26-37	487.91	11.45	−0.98	0.04	−5.83	24.91	0.11
	D26-33	165.77	3.05	−2.79	0.05	−3.32	27.50	0.15
	D26-30	247.66	3.84	−0.04	0.06	−8.01	22.67	0.13
Upper Gezhongwu	D26-28	346.90	2.92	−2.03	0.06	−4.90	25.87	0.11
	D26-25	839.22	18.55	−0.71	0.04	−7.13	23.57	0.07
	D26-23	215.79	3.53	−0.74	0.07	−7.64	23.04	0.13
	D26-19	191.52	2.65	−1.27	0.06	−6.82	23.89	0.10
	D26-17	276.04	4.71	−0.43	0.07	−11.07	19.51	0.16
	D26-15	505.20	11.05	0.36	0.05	−11.00	19.58	0.11
Lower Gezhongwu	D26-13	683.36	15.50	0.25	0.07	−11.05	19.53	0.09
	D26-11	442.37	9.32	−0.02	0.05	−10.28	20.32	0.10
	D26-7	1073.24	33.2	−0.58	0.06	−11.86	18.70	0.18
	D26-3	849.08	25.7	0.49	0.06	−10.96	19.62	0.10
	BD-12	93.87	17.00	1.08	0.06	−4.59	26.18	0.11
	BD-11	81.49	11.35	1.60	0.08	−5.26	25.49	0.07
	BD-10	26.86	21.94	0.70	0.06	−3.78	27.02	0.09
Upper Doushantuo	BD-9	10.17	18.95	1.07	0.06	−2.46	28.37	0.07
	BD-8	10.09	13.95	1.11	0.06	−1.53	29.33	0.12
	BD-7	117.53	38.77	−3.94	0.14	−10.06	20.54	0.31
	BD-6	133.35	37.68	−4.31	0.11	−10.84	19.73	0.38
	BD-4	256.84	33.46	−2.88	0.06	−8.50	22.15	0.16
Lower Doushantuo	BD-3	255.45	33.85	−3.30	0.05	−9.35	21.27	0.14
	BD-2	216.09	32.34	−3.08	0.05	−8.65	21.99	0.25
	BD-1	200.11	30.68	−2.41	0.06	−7.57	23.11	0.23

Gondwana, which would have enhanced continental denudation and provided continental materials (Reinhard et al., 2017; Wei et al., 2019). The total rates of continental weathering are paralleled by changes in the rates of biochemical continental weathering (Föllmi, 1996), which was depended on the atmospheric oxygen, which would be discussed in section 5.2. Furthermore, the $^{87}Sr/^{86}Sr$ of seawater increased gradually from Neoproterozoic to Cambrian (Kaufman et al., 1993; Stammeier et al., 2019), while

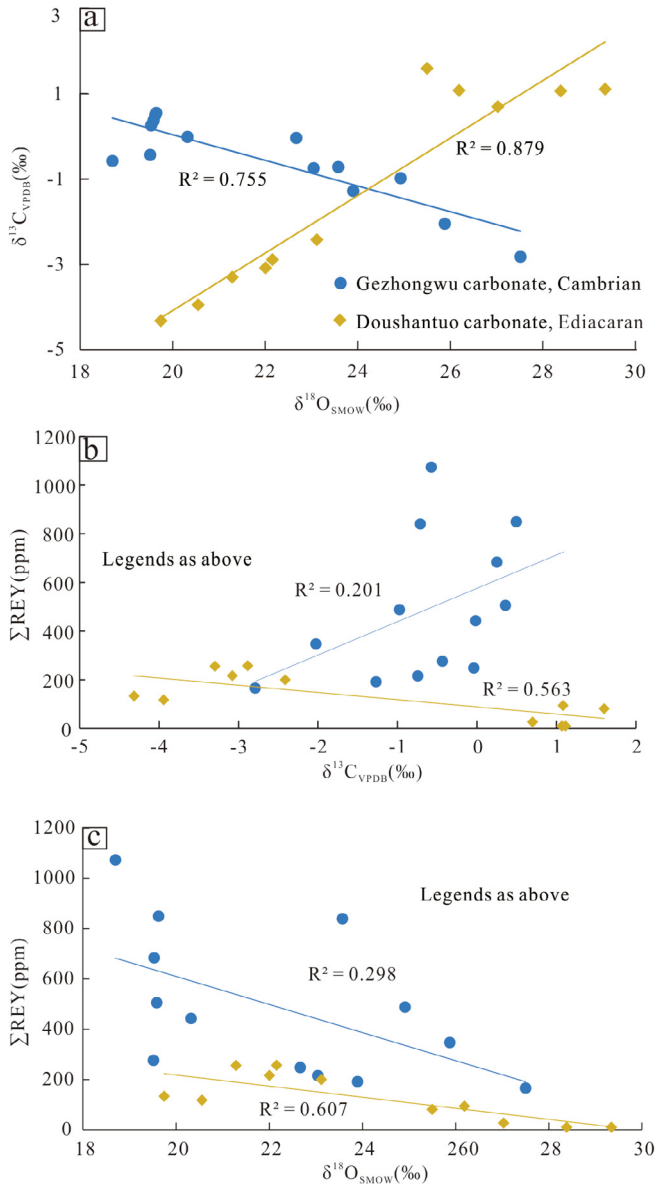

Fig. 10. Correlations among ∑REY of phosphorites and $\delta^{13}C_{VPDB}$ and $\delta^{18}O_{SMOW}$ of carbonate from Ediacaran and Cambrian, Central Guizhou.

ε_{Nd} just performed the reverse (Hu et al., 2016; Zhu and Jiang, 2017), consistent the worldwide seawater (Wei et al., 2013), which indicates the increased terrigenous flux. The higher P_2O_5 content of paleoland surfaces in West Sichuan and Central Yunnan (Yin et al., 2007a), as well as the higher SiO_2 and Al_2O_3 content in the phosphorites (Yang et al., 2019), also suggested delivery through weathering. Hence, post-glacial delivery through weathering and the corresponding P-rich upwelling would have provided the sources of P (Pufahl and Groat, 2017).

5.1.3. Potential sources of REY

In charge-and-radius-controlled geochemical systems, such as in pure melts, Y-Ho, and Zr-Hf pairs with similar charge and radius display highly coherent behaviors and retain their chondritic ratios (Bau, 1996). However, in aqueous systems, Y-Ho and Zr-Hf show non-chondritic characteristics (Bau et al., 1996). Y/Ho in sediment may result from, (i) the initial information of sources; (ii) Y and Ho fractionation in seawater; (iii) or transformation after precipitation.

Studies have shown that diagenetic processes cause Ce to become enriched and Dy_N/Sm_N to decrease, producing a negative correlation between Ce/Ce^* and Dy_N/Sm_N and a positive correlation between Ce/Ce^* and ∑REY (Morad and Felitsyn, 2001; Shields and Stille, 2001). In our study, none of these correlations was observed in the main samples (Fig. 8e, f, and 12a–d), except for the Upper Doushantuo phosphorite, suggesting that diagenetic alteration caused minimal REY fractionation. Moreover, in situ trace elemental composition showed that the difference between the Y/Ho ratios of authigenic phosphate and those of dolomite were insignificant (unpublished data), indicating that phosphogenesis caused none or only negligible Y/Ho differentiation. In Ediacaran phosphorite, the Y/Ho ratios in phosphate fractions (25.50–46.07) resemble that in carbonate fraction (25.43–49.74) (Xin et al., 2015). Thus, the Y/Ho alteration between phosphate and dolomite during diagenesis were limited.

As for the stronger surface complexation and weaker solution complexation of Y than Ho in seawater (Byrne and Kim, 1990), and the higher solubility product of $YPO_{4(s)}$ relative to $HoPO_{4(s)}$ (Byrne and Kim, 1993), Ho was preferentially scavenged relative to Y on condition that the Fe-Mn-(oxihydro)oxides or organic ligand were available in seawater (Bau et al., 1995; 1966; 1997). As discussed in 5.2, the seawater became oxygenated from the later Doushantuo to the Gezhongwu, and Fe-oxides (Fig. 6f, i) were found in Upper Doushantuo and Gezhongwu phosphorite. More-

Table 5
Apatite oxygen isotopes of the Doushantuo and Gezhongwu phosphorites from Central Guizhou.

Stratum	Sample No.	$\delta^{18}O_{P\text{-}SMOW}$ (‰)	$\delta^{18}O_{carb\text{-}SMOW}$ (‰)	$\Delta^{18}O_{CO_3\text{-}PO_4}$(‰)	∑REY (ppm)	P_2O_5 (wt.%)
Upper Gezhongwu	D26-37	15.7	24.91	9.21	487.91	11.45
	D26-33	14.9	27.50	12.60	165.77	3.05
	D26-30	14.4	22.67	8.27	247.66	3.84
	D26-28	11.1	25.87	14.77	346.90	2.92
	D26-25	16.0	23.57	7.57	839.22	18.55
	D26-23	16.7	23.04	6.34	215.79	3.53
	D26-19	17.0	23.89	6.89	191.52	2.65
Lower Gezhongwu	D26-17	18.9	19.51	0.61	276.04	4.71
	D26-15	18.0	19.58	1.58	505.20	11.05
	D26-13	16.1	19.53	3.43	683.36	15.50
	D26-11	14.6	20.32	5.72	442.37	9.32
	D26-7	17.7	18.70	1.00	1073.24	33.20
	D26-3	19.5	19.62	0.12	849.08	25.70
	D26-2	16.4	–	–	358.26	16.60
Upper Doushantuo	BD-11	15.0	22.15	10.50	81.49	11.35
	BD-10	15.8	21.27	11.23	26.86	21.94
	BD-8	17.5	21.99	11.84	10.09	13.95
Lower Doushantuo	BD-3	17.4	23.11	3.78	255.45	33.85
	BD-1	17.9	22.15	5.22	200.11	30.68

Note: $\Delta^{18}O_{CO_3\text{-}PO_4} = \delta^{18}O_{dol} - \delta^{18}O_P$.

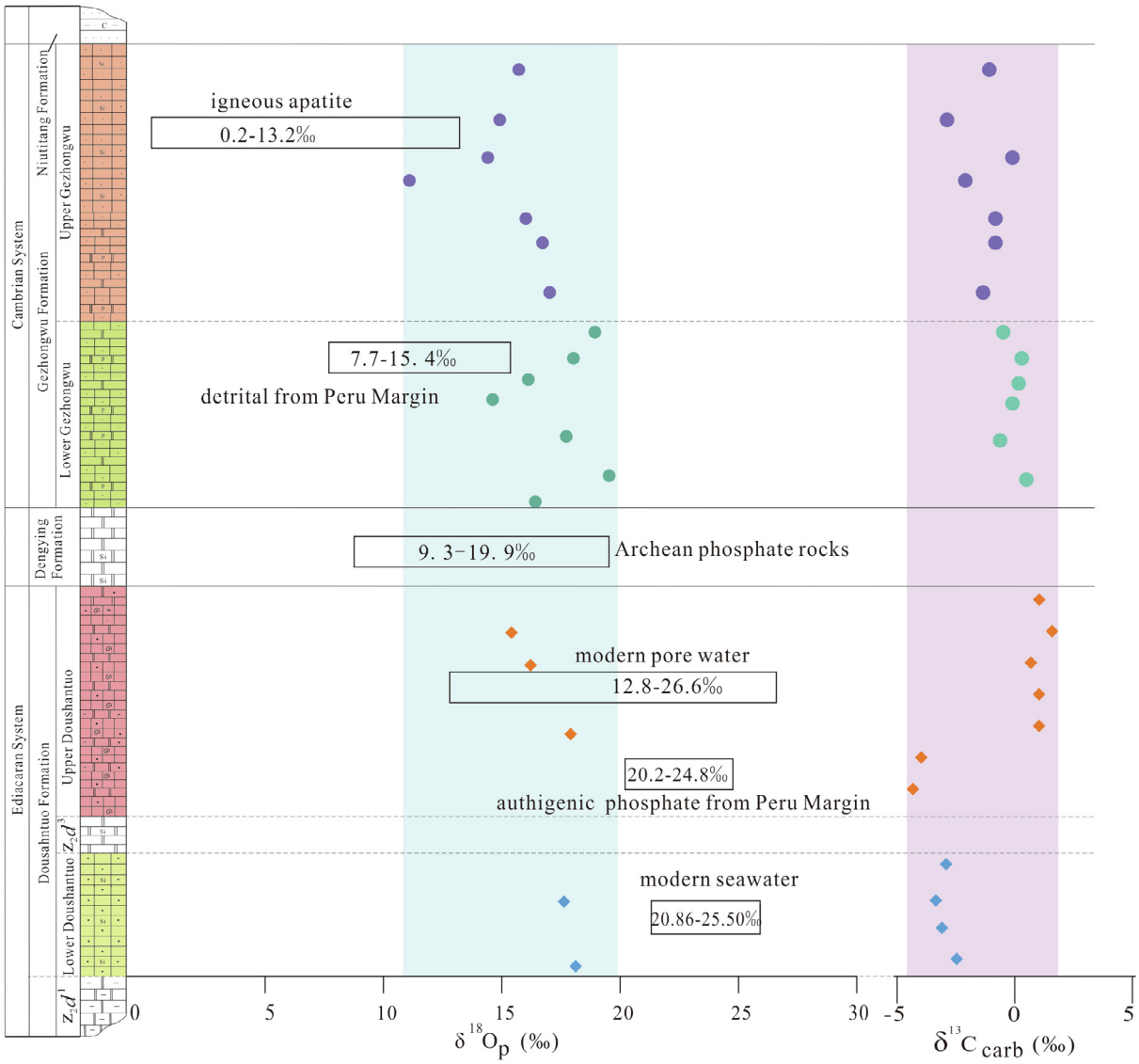

Fig. 11. Variation in $\delta^{18}O_p$ from the Doushantuo Formation, Ediacaran and Gezhongwu Formation, Cambrian. Igneous apatite data are from Mizota et al. (1992); detrital and authigenic phosphate data are from Jaisi and Blake (2010); modern seawater data are from Colman et al. (2005); pore water data are from Goldhammer et al. (2011a,b); Archean phosphate rock data are from (Blake et al., 2010).

over, petrographic characteristics (Fig. 6d-f, j-l) suggested that the microorganisms flourished in the later Doushantuo and the Gezhongwu. Generally, Fe-oxides and microorganisms might anticipate the fractionation between Y and Ho via preferential adsorption of Ho, resulting in the initial Y/Ho ratios were magnified. However, in our samples, the biogenic phosphorite of Upper Doushantuo had lower Y/Ho ratios than abiogenic phosphorite of Lower Doushantuo (Fig. 13). Excluding the diagenetic alteration in Y/Ho discussed above, this might because of REY sources with much lower Y/Ho ratios. Hence, when discussed the sources according to the Y/Ho ratios should take this factor into account.

Bau (1996) investigated the behaviors of Y, Ho, Zr, and Hf in different systems and summarized the Y/Ho and Zr/Hf ratios in some geological systems, suggesting that Y/Ho and Zr/Hf can be used to verify sources. In our Y/Ho–Zr/Hf binary diagram, all the samples were plotted beyond the end-members (Fig. 13) and the charge-and-radius-controlled area (Govindaraju, 1994), and all had Y/Ho ratios that were higher than those of igneous rocks and lower than those of seawater (Bau, 1996), indicating the mixing of marine facies deposition accompanied by terrigenous weathering products. Compared with the reported Y/Ho ratios of Ediacaran carbonate (36.8–49.5), shale 30.7–33.3 (Hu et al., 2016), and phosphate (25.50–46.07) (Xin et al., 2015) from Yangtze Platform, Doushantuo phosphorite had similar and homogeneous Y/Ho ratios, indicating a relatively stable and mixing source supply. Conversely, the Gezhongwu phosphorites had variable and lower Y/Ho ratios (15.95–52.77), indicating variable source input. Moreover, the Y/Ho ratios decreased from the Ediacaran to the early Cambrian overall (Fig. 13), consistent with $\delta^{18}O_p$, indicating the congenetic and mixed origins of P and REY. The positive correlations between P and ∑REY (Fig. 8a, b) provide further evidence of this. That the Zr/Hf ratios of all samples were between those of seawater and granites (Fig. 13) may also illustrate a mixed source, however, the Zr/Hf ratios were diversified by zircon minerals. The phosphorite from the Upper Doushantuo displayed variable Zr/Hf ratios (4.5–60.0), which were attributed to the input of detrital zircons during the late Doushantuo, as zircons were found under SEM (Fig. 6c).

The Y/Ho ratios of modern Pacific sediments were 24.7–28.7 (Paul et al., 2019), with minor fractionation during REY incorpora-

Table 6
The REE concentrations and Mo isotopic compositions of Doushantuo phosphorites and published Mo isotopes of Gezhongwu phosphorites.

Stratum	Sample No.	Rock type	∑REY (ppm)	Mo_{sample} (ppm)	Al (wt.%)	$Mo_{detritus}$ (ppm)	Mo_{EF} (ppm)	$\delta^{98/95}$Mo (‰)	2σ	
Upper Gezhongwu	GZW-02	dolomite	/	12.05	0.18	0.02	12.03	2.10	0.06	Data are according to (Liu, 2017)
	GZW-03	siliceous phosphorite	/	10.05	1.80	0.24	9.81	1.07	0.09	
	GZW-04	siliceous phosphorite	/	40.00	2.52	0.34	39.66	1.49	0.11	
	GZW-10	siliceous phosphorite	/	7.69	0.97	0.13	7.56	2.39	0.10	
	GZW-11	siliceous phosphorite	/	4.15	1.08	0.15	4.00	2.28	0.11	
	GZW-16	siliceous phosphorite	/	3.73	0.86	0.12	3.61	1.98	0.06	
Lower Gezhongwu	GZW-18	dolomite	/	0.55	0.46	0.06	0.49	2.16	0.08	
	GZW-22	dolomitic phosphorite	/	0.62	0.46	0.06	0.56	2.45	0.08	
	GZW-26	phosphorite	/	0.76	0.32	0.04	0.72	1.36	0.12	
	GZW-27	dolomitic phosphorite	/	1.05	0.12	0.02	1.03	1.57	0.05	
	GZW-30	phosphorite	/	1.11	0.3	0.04	1.07	1.51	0.05	
	GZW-31	dolomitic phosphorite	/	1.88	0.14	0.02	1.86	1.13	0.09	
	GZW-34	phosphorite	/	0.31	0.16	0.02	0.29	1.36	0.06	
	GZW-38	dolomitic phosphorite	/	0.19	0.17	0.02	0.17	1.29	0.14	
	GZW-39	dolomitic phosphorite	/	0.51	0.19	0.03	0.48	1.35	0.06	
	GZW-42	dolomitic phosphorite	/	0.26	0.14	0.02	0.24	2.37	0.08	
	GZW-43	phosphorite	/	0.31	0.16	0.02	0.29	1.80	0.05	
	GZW-48	dolomitic phosphorite	/	1.49	0.26	0.04	1.45	2.12	0.10	
Upper Doushantuo	BD-11	dolomitic phosphorite	84.92	0.13	0.12	0.02	0.11	−1.13	0.07	This study
	BD-8	dolomitic phosphorite	10.69	0.32	0.06	0.01	0.31	0.35	0.08	
	BD-6	dolomitic phosphorite	143.00	1.14	0.25	0.05	1.09	0.29	0.06	
	BD-5	dolomitic phosphorite	73.86	0.08	0.26	0.05	0.03	0.8	0.06	
Lower Doushantuo	BD-3	siliceous phosphorite	264.7	0.32	0.71	0.13	0.19	1.34	0.04	
	BD-1	siliceous phosphorite	211.07	0.41	1.09	0.20	0.21	0.70	0.03	

Notes: $Mo_{detrital} = [(Mo/X)_{upper\ crust}] \times X_{Sample}$ (after Rudnick and Gao, 2003); $Mo_{EF} = Mo_{sample} - Mo_{detrital}$.

tion into the phosphate in pore water (Reynard et al., 1999; Paul et al., 2019). The Ediacaran and early Cambrian phosphorite had higher and more variable Y/Ho ratios, which might be resulted by multiple source-rocks. The modern phosphorite in Namibian shelf had decreased Y/Ho ratios from the interiors (>50) to the exterior (~30) apatitic grains, furthermore, the Y/Ho ratios decreased with the increasing diagenesis (Lumiste et al., 2019). Even the decreasing Y/Ho ratios in modern apatitic grains were proved not suitable for paleoceanographic interpretation (Lumiste et al., 2019), it must be cautious when use REY to reconstruct paleoenvironment since the phosphate might be diagenetically influenced (Elderfield and Pagett, 1986; Reynard et al., 1999; Lumiste et al., 2019).

Hydrothermal fluids are considered as important sources of REY based on their positive Eu anomalies (Yang et al., 1997; Shi, 2005; Guo et al., 2017). Studies have shown that only under strongly acidic conditions can REY reach concentrations on the order of 10^{-3} (‰). Furthermore, many magmatic deposits have displayed pronounced REY migration (Li and Zhou, 2018) or formed rare earth ores with high economic value, such as the Bayan Obo carbonate-type REY deposit (Fan et al., 2005). Generally, REY belong to high field-strength elements, which migrated difficultly and occurred scarcely at low concentrations in most hydrothermal systems because REY are lost during boiling (Wood and Shannon, 2002). Research has indicated that Y and Ho may be fractionated in fluorine-rich hydrothermal fluids (Bau and Dulski, 1995), leading to extremely high Y/Ho ratios. In our study, samples were plotted far away from the hydrothermal area (Fig. 13), indicating that the REY contributions from hydrothermal fluids may be ignored.

5.1.4. High REY contents of Zhijin in Cambrian

As an attractive potential phosphorite-type REY deposit, the REY of Zhijin Cambrian phosphorite, South China, attract lot of research attention even though it is not mined with today's technology. According to the results shown in Fig. 13, it can be concluded that higher Y/Ho ratios might indicate a seawater source, while lower Y/Ho values likely imply terrestrial detrital input. In our samples, the negative correlation between Y/Ho and ∑REY (Fig. 8c, d), especially in Cambrian phosphorite, suggests that terrigenous weathering contributed the major REY rather than the terrigenous weathering materials. In previous studies, it was reported that the Proterozoic igneous rocks of South China had similar Y/Ho values to those of the Gezhongwu phosphorites, including the magmatites of the Xixiang Group (~1013 ± 16 Ma) from Shanxi Province (Y/Ho = 27.37–29.23, mean: 28.20) (Gao et al., 1996) and the magmatites of the Xionger Group (1840 ± 14 Ma) from Henan Province (Y/Ho = 25–27.27, mean: 26.13) (Gao et al., 1996). These might be the potential sources for the high REY in the early Cambrian ocean, providing a possible explanation for Zhijin phosphorites becoming enriched in REY with increased continental weathering rates and subsequent contribution to shallow waters.

The observed variation in $\delta^{13}C_{carb}$ from the Ediacaran to the Cambrian was consistent with previously reported data and global marine carbonates from the Late Proterozoic, remaining near −2‰ to −4‰ during the Varanger Glaciation and then increasing to 4‰ to 5‰, remaining at 2‰ until the Cambrian (Kaufman and Knoll, 1995). However, $\delta^{13}C_{carb}$ from different sections showed spatial variations across the shelf-basin transects in the South China (Guo et al., 2007; Jiang et al., 2007, 2011; Ader et al., 2009). Which might result from the burial diagenesis (Knauth and Kennedy, 2009; Derry, 2010) or absence of precise radiometric age data (Derry, 2010). Even lack a reasonable explanation for the variation mechanism, $\delta^{13}C_{carb}$ remains critical to establish the globally time-equivalent and record the isotopic signature (Jiang et al., 2011). Research has shown that, when microorganisms die under anoxic conditions, increased organic carbon burial scavenges ^{12}C from seawater, causing a relative enrichment of ^{13}C. Conversely, under oxic conditions, OM is degraded, leading to ^{12}C enrichment in seawater, which is recorded in carbonates (Canfield et al., 2007). The positive $\delta^{12}C_{carb}$ excursion in the lower part of the Upper Doushantuo (Fig. 7) may be related to enhanced biological productivity (Delaney, 1989), which is consistent with the abundance of microfossils. Meanwhile, in the $\delta^{13}C-\delta^{18}O$ binary diagram, the $\delta^{13}C$ was plotted with marine carbonates and showed little inclination toward sedimentary OM (Fig. 14), indicating that marine carbonate

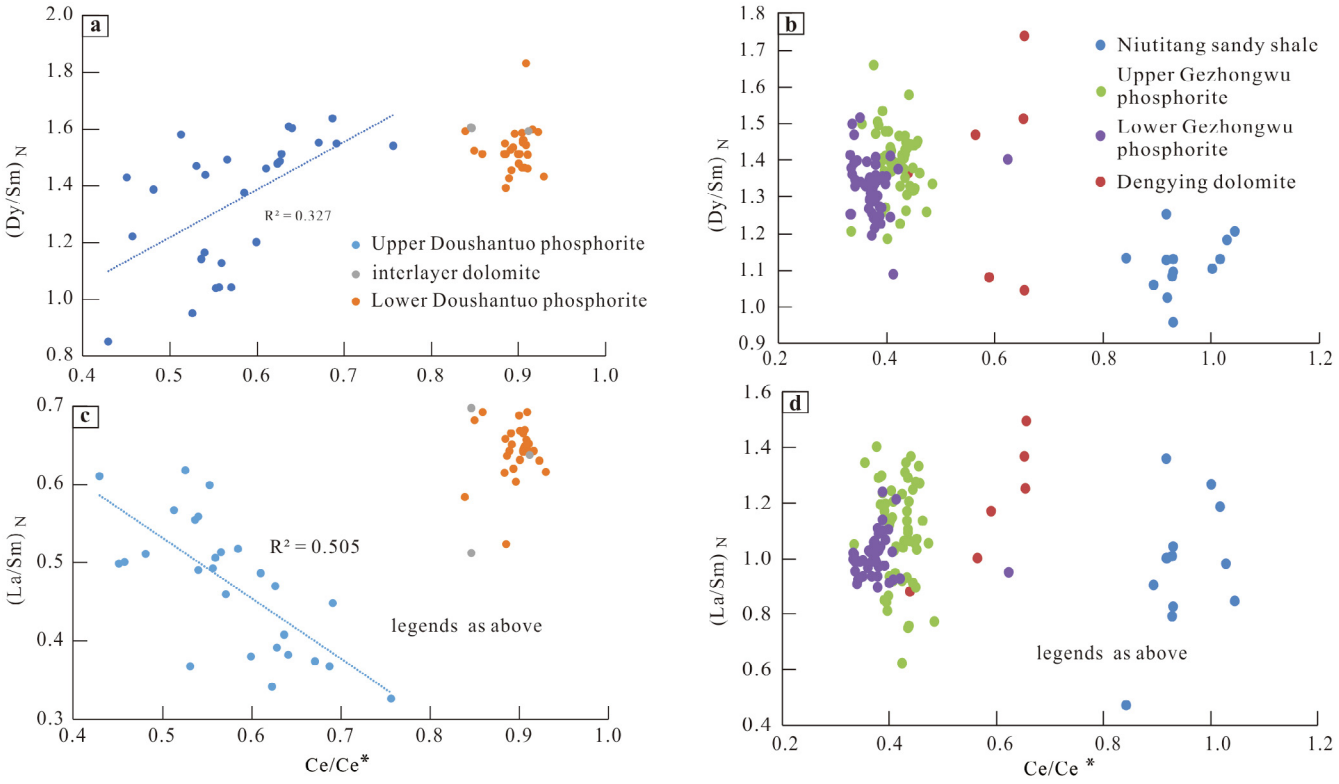

Fig. 12. Relationships between the Ce_{anom} and Dy_N/Sm_N (a, b) and between Ce_{anom} and La_N/Sm_N (c, d) of the phosphorites from Central Guizhou.

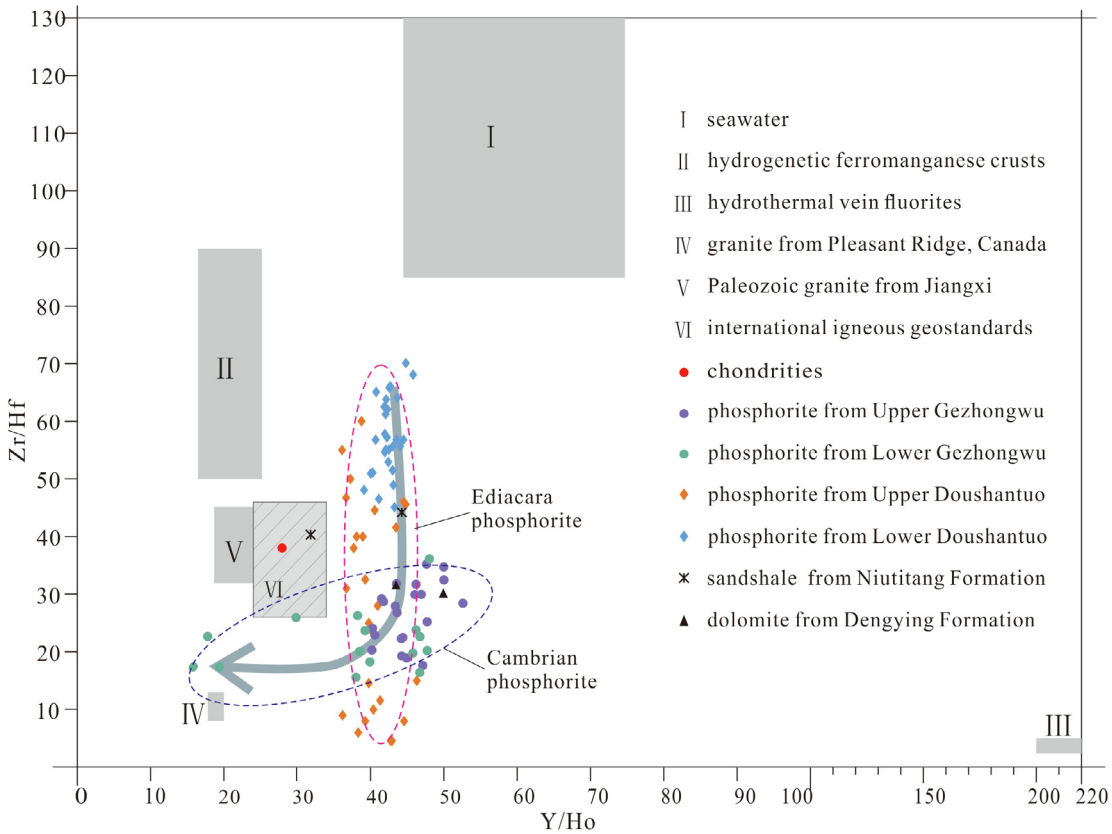

Fig. 13. The Y/Ho and Zr/Hf binary diagram of Doushantuo phosphorite, Ediacaran and Gezhongwu phosphorite, Cambrian. Data for (I) from Zhang et al. (1994), (II) from Bau (1996) and Bau and Dulski (1996), (III) from Bau and Dulski (1995), (IV) from Taylor (1992), (V) from Feng et al. (2014), (VI) from Govindaraju (1994). The arrow represents the variation tendency of Y/Ho and Zr/Hf ratios of phosphorite from Lower Doushantuo to Upper Gezhongwu.

precipitation was contributed by seawater but not by the organic carbon or igneous carbonates.

Furthermore, the $\delta^{13}C_{carb}$ might provide source evidence of high ∑REY in Zhijin Cambrian phosphorite. The $\delta^{13}C_{carb}$ will exhibit coordinated variation with $\delta^{13}C_{org}$, regardless of the fractionation mechanism, and was widespread in the late Proterozoic carbonates (Kaufman and Knoll, 1995). However, there were two negative excursions of $\delta^{13}C_{org}$ and $\delta^{13}C_{carb}$ plotted along the boundary of the Doushantuo and Dengying formations and the PC/C boundary (Lambert et al., 1987; Yang et al., 1999; Wang, 2010), which resulted in the existence of dissolved organic carbon (DOC) enriched in ^{12}C in the deepsea (Fike et al., 2006; Jiang et al., 2007; Wang, 2010). Moreover, the presence of ^{13}C-depleted deep-water carbonates and the strong surface-to-deep ocean $\delta^{13}C_{carb}$ gradient in the Ediacaran ocean (Jiang et al., 2007) indicate the existence of DOC. Along with glacial melting, deep seawater rich in ^{12}C was upwelled to the shallow sea (Kaufman and Knoll, 1995; Mi, 2010). Hence, the positive correlations between ∑REY and $\delta^{13}C_{carb}$ in the Gezhongwu carbonate (Fig. 10b) and nearly every REY enrichment responded to the positive $\delta^{13}C_{carb}$ excursion (Fig. 7), indicating that the deep seawater brought few REY. Conversely, terrigenous weathering might have served as the primary source of REY in Zhijin Cambrian ocean.

Even though abundantly provided by terrigenous weathering materials, the high REY content of Zhijin Cambrian phosphorite might controlled by other factors. Ilyin (1998) studied the world Vendian–Early Cambrian phosphorite and suggested that pelletal phosphorites with higher surfacer/mass ratios had higher REE content than that of structureless phosphorites with lower surfacer/mass ratio. Granular or pelletal phosphorites are believed to have been underwent diagenetic process (Riggs, 1979), hence, granules contacted with seawater for a long period, promoting diagenetic enrichment in REE (Ilyin, 1998). Zhang et al. (2003) studied the Zhijin phosphorite and proposed that the biological–chemical sediment control the absorption of REY into phosphate based on plenty of biodetritus and high REY content. Furthermore, the sedimentary facies control the REY content in phosphorite, it was hard for P and REY to be formed in the upper slope facies and upper slope facies, while the shallow water ramp facies were benefitial for high REE bearing phosphorous deposits (Chen et al., 2013). All these factors were benefitial for Zhijin phosphorite, the coefficient of these factors, combined with the abundant sources, resulting the REE-rich phosphorite in Zhijing during Cambrian.

5.2. Redox conditions

The geochemical properties of Ce are the same as those of other lanthanides in anoxic seawater. While in oxic marine environments, soluble Ce^{3+} is oxidized into insoluble Ce^{4+} and suspended in the water as CeO_2, fractionating with other lanthanides and resulting in strongly negative Ce anomalies in coeval sediments (Holser, 1997; Pourret et al., 2008). McArthur and Walsh (1984) suggested that negative Ce anomalies in seawater could be inherited by francolites formed under oxic seawater conditions. Generally, Ce_{anom} values less than −0.1 reflect oxic conditions, and values greater than −0.1 reflect anoxic conditions (Haskin et al., 1968). The Ce_{anom} of phosphorites from the Lower Doushantuo and interbedded dolomite were greater than −0.1, whereas the phosphorites of the Upper Doushantuo, Dengying dolomites, Lower Gezhongwu phosphorites, and Upper Gezhongwu phosphorites all had Ce_{anom} values less than −0.1, which means that the seawater transformed to oxic in the late Doushantuo until the Gezhongwu Formation was deposited. There being no correlations between Ce/Ce* and ∑REY (Fig. 8e, f), and Ce/Ce* and Dy_N/Sm_N (Fig. 12a, b) suggest that diagenetic alteration minimally affected the Ce anomaly and that the Ce anomaly recorded the primary environment during phosphorite formation. Therefore, Ce anomalies can reflect the original redox conditions of phosphate formation in the studied sediments. These results were consistent with previous studies (Wu et al., 1999, 2006; Xie et al., 2003; Shi et al., 2004; Zhang et al., 2004; Yang et al., 2019).

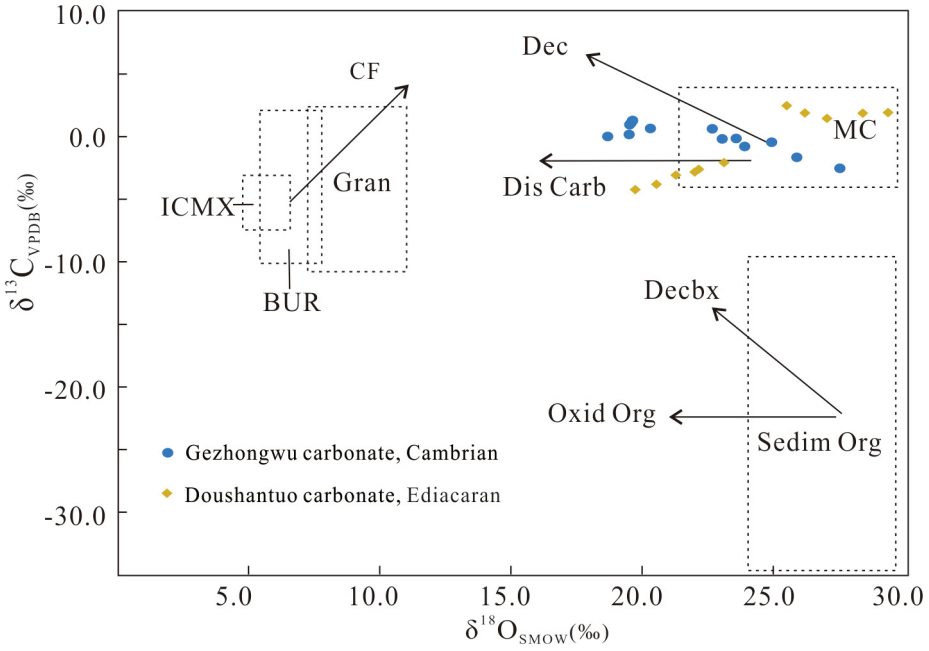

Fig. 14. Binary diagram of $\delta^{13}C_{VPDB}$ and $\delta^{18}O_{SMOW}$ for carbonates from the Ediacaran Doushantuo and Cambrian Gezhongwu formations of Central Guizhou. The base map is from Liu and Liu (1997). Abbreviations: MC, marine carbonate; Dec, decarbonation; Dis Carb, carbonate dissolution; Decbx, decarboxylation; Oxid Org, organic matter oxidation; Sedim Org, sedimentary organic matter; Gran, granite, ICMX, igneous carbonate and mantle xenoliths; BUR, basic/ultrabasic rock; CF, crystal differentiation.

Studies have suggested that Mo isotopic fractionation mainly depends on the redox conditions, while it does not respond overtly to pH, temperature, or biological activity. As with the petrographic characteristics described above, the Lower Doushantuo phosphorite contained many pyrites (Fig. 6b), and the Ce_{anom} was greater than –0.1 (Supplementary data, Table S2), indicating anoxic conditions. The content of SO_2 and TFe_2O_3 for Lower Doushantuo were higher than that of Upper Doushantuo, even as high as 3.47% and 3.41%, respectively, implying anoxic and sulfidic condition during Lower Doushantuo formed. Under these conditions, MoO_4^{2-} reacts with H_2S and generates thiomolybdate, causing Mo isotopic fractionation characterized by the isotopically lighter products and heavier reactants (Erickson and Helz, 2000; Tossell, 2005; Nägler et al., 2011). Once the thiomolybdate precipitated immediately in the seawater, Mo isotopic fractionation was restricted and the Mo isotopes of seawater were recorded by these sediments (Nägler et al., 2011; Noordmann et al., 2015). Considering the rapid sedimentation rate of Mo under anoxic and sulfurized condition (Fan et al., 2007), the $\delta^{98/95}$Mo of the Lower Doushantuo could represent the value of contemporaneous seawater. Furthermore, studies have shown that scarcely any sediments have $\delta^{98/95}$Mo values higher than contemporaneous seawater (Anbar, 2004; Anbar and Rouxel, 2007), therefore, the $\delta^{98/95}$Mo of sediments is regarded as the prescribed minimum of seawater (Barling et al., 2001; Siebert et al., 2003; Wille et al., 2008; Wen et al., 2010, 2011). Lower Doushantuo phosphorites had heaviest $\delta^{98/95}$Mo values 1.34‰, suggesting that the heaviest $\delta^{98/95}$Mo of Ediacaran ocean had ever reached values at least 1.34‰, which is heavier than the reported $\delta^{98/95}$Mo in the Proterozoic ocean (−0.12‰ to 1.20‰) (Arnold et al., 2004). These findings reflect that the seawater in Central Guizhou tended to be oxygenated since the early Doushantuo, Late Neoproterozoic.

In the Upper Doushantuo phosphorite, the $\delta^{98/95}$Mo decreased gradually and even had a negative $\delta^{98/95}$Mo (−1.13‰) excursion at the top of the Doushantuo Formation. The highly negative Ce anomalies (Supplementary data, Table S2) and plenty of microorganism fossils (Fig. 6d–f) in the Upper Doushantuo indicate oxic conditions. Under these conditions, MoO_4^{2-} was soluble, while isotopically lighter Mo was scavenged by $Mo(OH)_6$, resulting in isotopically heavier seawater (You et al., 1986; Erickson and Helz, 2000). Even though the phosphorites have the potential to record the Mo isotopes of paleo-oceans, the influence of Fe- and Mn-oxides and diagenetic reformation might change the Mo isotopic composition (Wen et al., 2011). Since the Upper Doushantuo phosphorite contained many Fe-oxides and metasomatic forms (Fig. 6e, f), we speculated that the lighter $\delta^{98/95}$Mo in the Upper Doushantuo might result from the isotopically lighter Mo adsorption by Fe-oxides or diagenesis. Another reason might be the lighter Mo input along with upwelling or weathering (Siebert et al., 2003).

All Gezhongwu phosphorites have heavier Mo isotopic values than those of Doushantuo phosphorite, and the $\delta^{98/95}$Mo of Gezhongwu phosphorite is close to that of modern seawater (~2.34‰ ± 0.10‰) (Barling et al., 2001; Siebert et al., 2003), which demonstrates that the Cambrian seawater was completely oxic in Central Guizhou. The multiple isotopic variations in Lower Gezhongwu phosphorites might have been caused by turbulent seawater or the different proportions of Mo sources. The Lower Gezhongwu phosphorite had lighter Mo isotopes than those of Upper Gezhongwu phosphorite, resulting from the isotopically lighter Mo adsorption by Fe-oxides in the Lower Gezhongwu (Wen et al., 2011; Liu, 2017). Furthermore, as anoxic and sulfidic conditions benefit Mo precipitation more than oxic conditions, the higher Mo content of the Upper Gezhongwu (3.73–40.00 ppm) than Lower Gezhongwu (0.19–1.49 ppm) indicated that the seawater in the Lower Gezhongwu was relatively more oxic than that of the Upper Gezhongwu (Liu, 2017). These characteristics are consistent with petrographic characteristics, confirming a more stable and deeper seawater in the Upper Gezhongwu than that in the Lower Gezhongwu.

The redox conditions recorded by Ce anomalies and Mo isotopic compositions were consistent with the Neoproterozoic Oxygenation Event (Och and Shields-Zhou, 2012; Pufahl and Hiatt, 2012), during which oxygen levels have increased substantially. It is doubtless that atmospheric oxygen played an important role in seawater redox evolution during the Ediacaran-Cambrian transition (Fan et al., 2014, 2016; Han and Fan, 2015). Studies implied that atmospheric O in the Late Ediacaran was estimated as 8% to 40% of the present atmospheric level (Canfield et al., 2007; Butterfield, 2009), whereas Cambrian had higher atmospheric O than that of Proterozoic (Knoll and Carroll, 1999; Berner et al., 2003) and the early Cambrian oceans had oxygen levels close to those of the modern ocean (Li et al., 2010; Guilbaud et al., 2018). Rising oxygen levels are thought to have led to the extend oxygenation of seawater (Berner, 2006; Och and Shields-Zhou, 2012; He et al., 2019). However, it is difficult to determine the atmospheric oxygen increase mechanism during this period. Widespread orogeny enhanced continental denudation, hence, plentiful nutrient export to continental marginal seawater (Reinhard et al., 2017), enhancing the primary productivity (Wei et al., 2019). As a result, the burial of pyrite and organic carbon during Ediacaran-early Cambrian oceans released large amounts of O_2 to the ocean and atmosphere (He et al., 2019; Li et al., 2020), as well as the P scavenging and N-fixation (Reinhard et al., 2017). Hence, the positive feedback between oxygen levels in atmosphere and primary productivity caused progressive oxygenation of earth's ocean–atmosphere system. The oxygenation of seawater extended from the surface to the bottom in the Ediacaran ocean (Goldberg et al., 2007; Fan et al., 2014, 2016), resulting in oxic conditions by the end of the Ediacaran and continuously extended oxygenation in the Cambrian in Central Guizhou.

The role of oxygen in the origins of animals has been heavily debated (Canfield et al., 2007; Lyons et al., 2014; Zhang et al., 2014; Fox, 2016). The oxygenation of the Ediacaran ocean facilitated the diversification of eukaryotic life (Awramik et al., 1985; Knoll, 2000; Fan et al., 2016), as the same for "Cambrian explosion" (Cai et al., 2019; Knoll and Carroll, 1999; Zhang et al., 2014). Previous studies suggested that the Ediacaran fossils were divided into algal microorganisms (Xiao and Knoll, 1999, 2000; Zhou et al., 2007), animal embryos (Cunningham et al., 2017; Xiao et al., 1998; Yin et al., 2007b), and their larval and adult forms (Cunningham et al., 2017), belonging to simple animals. While there were abundant diverse shelly fossils in the basal Cambrian (Cai et al., 2019; Zhuravlev and Wood, 2018), and the "Cambrian explosion" produced more complex kinds of animal common today, such as arthropods and chordates (Butterfield, 2009; Fox, 2016). Recent research suggested the evolution between Ediacaran and Cambrian animals was continuous (Cai et al., 2019). Fox (2016) believed the complex types in Cambrian need more oxygen than these of Ediacaran, hence, oxygen might be one of key triggers for the evolutionary explosion (Knoll and Carroll, 1999; Marshall, 2006). However, besides the oxygen content in the biogeology systerm, global and regional temperature dynamics, food provided to early animals, and other environment changes were also important for animal evolution (Zhang et al., 2014; Sperling and Stockey, 2018; He et al., 2019).

5.3. Formation mechanism

The formation of marine sedimentary phosphorite were closely related to redox conditions (Heggie et al., 1990; Pufahl and Grimm, 2003; Pufahl and Groat, 2017). Since the anoxic seawater in the early Doushantuo prevented infaunal colonization, abiological

and bedded phosphate lithofacies developed (Pufahl and Groat, 2017) under strong mechanical power (Zhang et al., 2019), which was supported by the petrographic characteristics (Fig. 5a, i and 6a–c). Abiological phosphorites formed through two ways. One took place only under steady hydrodynamics, P-bearing sediments underwent the consolidation and phosphatization after precipitation and was less broken, forming blocky phosphate (Fig. 6c). Another took place via rework process under strong mechanical power. Plenty of transgressions occurred after the Marinoan glaciation in Central Guizhou, providing both origins of P and mechanical

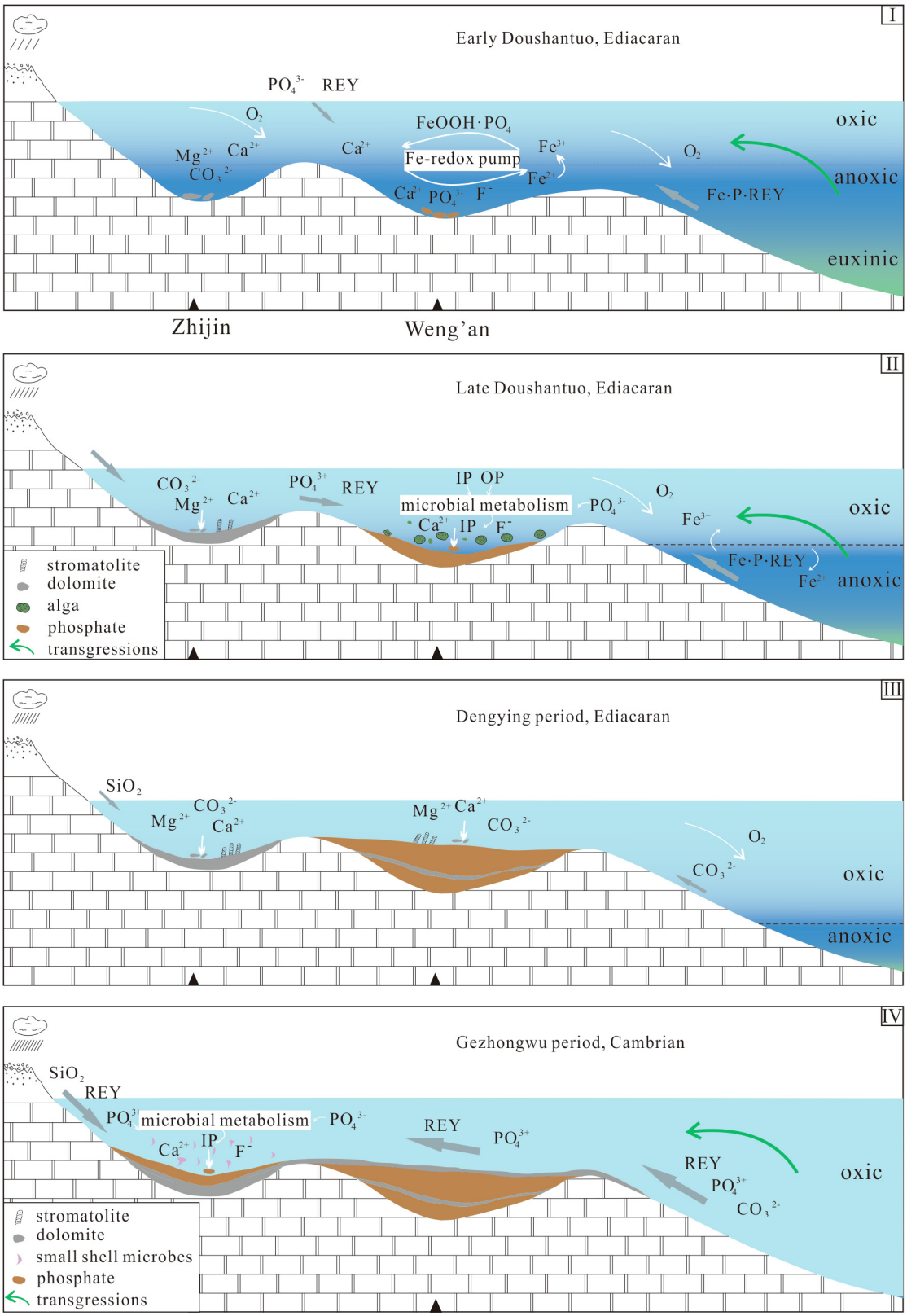

Fig. 15. Diagram of phosphorite metallogenesis from the Ediacaran to the early Cambrian in Central Guizhou.

power. Under these turbulent waters, the previously precipitated phosphate was separated and rounded under the strong mechanical power of seawater (Föllmi, 1996; Zhang et al., 2016). The globular intraclasts (Fig. 6a, g-h), similar to the "coated grains" (Pufahl and Grimm, 2003), are thought to form via multiple episodes of phosphogenesis and reworking of existing phosphatic sediments (Pufahl and Grimm, 2003; Zhang et al., 2019). Furthermore, the horizontal bedding (Fig. 5i), high psephicity (Fig. 6a, g) and reworked structures (Fig. 6e, h) supported the reworked process under conditions with high-energy condition (Liu et al., 1987; Zhang et al., 2019) resulted by storm-wave winnowing and subsequent rounding (Soudry, 1992; Zhang et al., 2019).

During the late Doushantuo and Gezhongwu times, seawater was oxygenated and plenty of microorganisms flourished (Fig. 6-d-f, j-l), biogenetic and reworked phosphorite formed (Fig. 5e, f, h, j). The transition of redox conditions could not be the direct reason for the phosphogenic event but can be responsible for the genetic mechanism transition of phosphorite (Yang et al., 2019). Phosphatized microfossils indicated that microorganism participated the phosphgenesis. Well-preserved algal microorganisms (Fig. 6d, f) and animal embryos (Fig. 6e) indicated the phosphatisation and compression occurred after the buried of microorganisms (She et al., 2013; Muscente et al., 2015; Yang et al., 2019). Doushantuo algal- and embryo-like fossils (Fig. 6d–f) and the Gezhongwu shelly fossils (Fig. 6j–l) record the accretionary growth of microorganisms in a certain extent (She et al., 2013; Yang et al., 2019). Partially broken algal microfossils indicated that algal microorganisms may have been degraded prior to final burial (Muscente et al., 2015). During the process, bacterial participate in the degradation of microorganisms (Arning et al., 2009; She et al., 2013), resulting in the P release into pore wate (Yang et al., 2019). Indeed, partial phosphatized fossils are reworked and secondarily-concentrated bioclasts prior to final burial (Xiao and Knoll, 1999; Muscente et al., 2015). The microorganisms in the Gezhongwu Formation were better preserved than those of the Doushantuo, indicating a calmer depositional environment or faster precipitate rate during Cambrian.

5.4. Phosphogenic model

According to the origins of ore-forming materials, redox conditions, and formation mechanisms analyzed above, we developed a phosphogenic model that explains how these two phosphorite deposits were formed within only a few myrs (Fig. 15) around the PC/C boundary. In the ocean, P is removed predominantly by organisms (Froelich et al., 1988; Yuan et al., 2019), partially via the sorption to Fe-(oxy)hydroxides (Berner, 1973) and authigenic mineral formation (Ruttenberg and Berner, 1993). In early Doushantuo, the thawing of the Marinoan glaciers caused transgressions, bringing abundant P through the adsorption of iron hydroxides (FeOOH) (Shaffer, 1986) into the shallow sea area (Fig. 15-II). During this time, the seawater was stratified by oxic surface waters and anoxic bottom waters in Weng'an, which enabled phosphate precipitation via the Fe-redox pump (Cappellen and Berner, 1988; Jiang et al., 2011; Pufahl and Hiatt, 2012). When the $FeOOH{\cdot}PO_4^{3-}$ ionic group entered the anoxic sediment–water interface, Fe^{3+} was reduced to Fe^{2+}, and PO_4^{3-} was released into the sediments (Cappellen and Berner, 1988; Jiang et al., 2011; Pufahl and Hiatt, 2012). Subsequently, phosphorite was formed through the reworking of previous phosphatic sediments by mechanical power; a detailed description was given by Yang et al. (2019).

In the late Ediacaran, the seawater was gradually oxygenated, and microorganisms began to flourish, resulting in many algae and animal embryo fossils (Fig. 15-II). Both weathering and deep seawater contributed P and REY in varying proportions, and P was immediately metabolized once microbial mats existed in the water. The microorganism absorbed P and other matters for growth. During nutriment (P)-depleted stages, microorganisms died and precipitated into water–sediment interface. After phosphate precipitation, partial algal microorganisms were degraded by bacteria, and P was released into porewater. Meanwhile, buried P was redistributed among organic and inorganic P phases during post-depositional and diagenetic processes, ultimately forming the phosphatic fossils (Fig. 6d-f) and amorphous apatite (Fig. 6e). In Dengying times, dolomite was formed due to the decreased transgression and P/REY source limitation (Fig. 15-III).

Along with the extension of oxygenation from the surface seawater to the bottom, the conditions in the Cambrian remained oxic and many small shelly organisms evolved in Zhijin (Fig. 15-IV). The small shelly organisms adsorbed P and REY for growth in seawater, resulting in the rapid exchange of oxygen between PO_4^{3-} and H_2O during biological reactions, which are generally complete within a few days to weeks (Stout et al., 2014). The dissolved inorganic P released by metabolism, irrespective of the source, could precipitate into sediments, and microorganisms could be buried rapidly after death, undergoing limited degradation. Phosphatization occurred in sediments, forming phosphatic fossils via the resembling process in the early Doushantuo. The enzyme-catalyzed hydrolysis of organic debris and subsequent release of P has been found to be an important pathway for authigenic P minerals (Ruttenberg and Berner, 1993).

6. Conclusions

Phosphogenesis from the Ediacaran to early Cambrian was closely related or even continuous in sources, redox evolution, animal evolution, and formation mechanism of phosphorite.

After the Marinoan glaciation, post-glacial weathering delivery and corresponding P-rich upwelling would have provided the sources of P and REY into South China. The decreased $\delta^{18}O_p$, Y/Ho, and Zr/Hf overall from the Ediacaran to early Cambrian indicated increased weathering delivery in the Cambrian than in the Neoproterozoic, while seawater delivery concomitantly declined. Furthermore, increased terrigenous weathering delivery responding to a series of geodynamic changes significantly elevated marine REY concentrations in the Cambrian in Zhijin.

The positive feedback between oxygen levels in atmosphere and primary productivity caused progressive oxygenation in ocean–atmosphere system, which played an important role in seawater redox evolution during the Ediacaran-early Cambrian transition. The result was that the seawater transformed from anoxic to oxic in the late Doushantuo and was entirely oxic during the Cambrian in Central Guizhou. The redox evolution might trigger the animal evolutionary from simple Ediacaran-type to complex Cambrian explosion and enabled phosphorites to be formed by different mechanisms.

Based on the origins, redox conditions, and formation mechanisms, a phosphogenic model of Ediacaran to early Cambrian phosphorite formation was established. Wherein the Lower Doushantuo phosphorites formed via the reworking of preexisting phosphatic sediments under strong mechanical power of seawater, while Upper Doushantuo and Gezhongwu phosphorites formed via microbial metabolism and burial alteration. Although further validation is needed, this model may proved useful when confirming the specific origins by more evidence and examining the effects of early Earth redox transformations on seawater and sedimentary chemistry, as well as biological evolution.

Declaration of Competing Interest

The authors declare that they have no known competing financial interests or personal relationships that could have appeared to influence the work reported in this paper.

Acknowledgments

The authors are grateful to Prof. Peir K. Pufahl, Prof. Hui Zhang, Prof. Xingchun Zhang, and Prof. Hanjie Wen for their helpful suggestions toward improving the quality of this manuscript. This work was supported by the United Foundation of National Natural Science Foundation of China (Grant Numbers: 41972095, U181240004, 9206220039) and the Public Beneficial, Basic Geological Project of Department of Land and Resources of Guizhou Province (Grant Number: 2016-09-1).

Appendix A. Supplementary data

Supplementary data to this article can be found online at https://doi.org/10.1016/j.gsf.2021.101187.

References

Ader, M., Macouin, M., Trindade, R.I.F., Hadrien, M.H., Yang, Z., Sun, Z., Besse, J., 2009. A multilayered water column in the Ediacaran Yangtze platform? Insights from carbonate and organic matter paired delta C-13. Earth Planet Sci. Lett. 288, 213–227.

Anbar, A.D., 2004. Molybdenum stable isotopes: observations, interpretations and directions. Rev. Mineral Geochem. 55, 429–454.

Anbar, A.D., Rouxel, O., 2007. Metal Stable Isotopes in Paleoceanography. Annu. Rev. Earth P. L. Sc. 35, 717-746.

Angert, A., Weiner, T., Mazeh, S., Sternberg, M., 2012. Soil phosphate stable oxygen isotopes across rainfall and bedrock gradients. Environ. Sci. Technol. 46, 2156–2162.

Arning, E.T., Lückge, A., Breuer, C., Gussone, N., Birgela, D., Peckmann, J., 2009. Genesis of phosphorite crusts off Peru. Mar. Geol. 262, 68–86.

Arnold, G.L., Anbar, A.D., Barling, J., 2004. Molybdenum isotope evidence for widespread anoxia in Mid-Proterozoic oceans. Science 304, 87–90.

Awramik, S.M., McMenamin, D.S., Yin, C.Y., Zhao, Z.Q., Ding, Q.X., Zhang, S.S., 1985. Prokaryotic and eukaryotic microfossils from a Proterozoic/Phanerozoic transition in China. Nature 315, 655–658.

Barling, J., Arnold, G.L., Anbar, A.D., 2001. Natural mass-dependent variations in the isotopic composition of molybdenum. Earth Planet Sci. Lett. 193, 447–457.

Bau, M., 1996. Controls on the fractionation of isovalent trace elements in magmatic and aqueous systems: evidence from Y/Ho, Zr/Hf, and lanthanide tetrad effect. Contrib. Mineral Petr. 123, 323–333.

Bau, M., Dulski, P., 1995. Comparative study of yttrium and rareearth element behaviours in fluorine-rich hydrothermal fluids. Contrib. Mineral Petr. 119, 213–223.

Bau, M., Dulski, P., 1996. Distribution of yttrium and rare-earth elements in the Penge and Kuruman iron-formations, Transvaal Supergroup, South Africa. Precambrian Res. 79, 37–55.

Bau, M., Dulski, P., 1999. Comparing yttrium and rare earths in hydrothermal fluids from the Mid-Atlantic Ridge: implications for Y and REE behaviour during near-vent mixing and for the Y/Ho ratio of Proterozoic seawater. Chem. Geol. 155, 70–90.

Bau, M., Dulski, P., Möller, P., 1995. Yttrium and holmium South Pacific seawater: vertical distribution and possible fractionation mechanisms. Chem. Erde-Geochem. 55, 1–16.

Bau, M., Koschinsky, A., Dulski, P., Hein, J.R., 1996. Comparison of the partitioning behaviours of yttrium, rare-eatrh elements, and titanium between hydrogenetic marine ferromangaese crust ans seawater. Geochim. Cosmochim. Acta 60, 1709–1725.

Bau, M., Möller, P., 1992. Rare earth element fractionation in metamorphogenic hydrothermal calcite, magnesite and siderite. Miner. Petrol. 45, 231–246.

Bau, M., Möller, P., Dulski, P., 1997. Yttrium and lanthanides in eastern Mediterranean seawater and their fractionation during redox-cycling. Mar. Geol. 56, 123–131.

Berner, R.A., 1973. Phosphate removal from sea water by adsorption on volcanogenic ferric oxides. Earth Planet Sci. Lett. 18, 77–86.

Berner, R.A., 2006. GEOCARBSULF: A combined model for Phanerozoic atmospheric O_2 and CO_2. Geochim. Cosmochim. Acta 70, 5653–5664.

Berner, R. A., Beerling, D. J., Dudley, R., Robinson, J. M.,Wildman, R. A., 2003. Phanerozoic atmospheric oxygen. Annu. Rev. Earth P. L. Sc. 31, 105-134.

Blake, R.E., Chnag, S.J., Lepland, A., 2010. Phosphate oxygen isotopic evidence for a temperate and biologically active Archaean ocean. Nature, 1029–1032.

Blake, R.E., O'Neil, J.R., Garcia, G.A., 1997. Oxygen isotope systematics of biologically mediated reactions of phosphate: I. Microbial degradation of organophosphorous compounds. Geochim. Cosmochim. Acta 61, 4411–4422.

Blake, R.E., O'Neil, J.R., Surkov, A.V., 2005. Biogeochemical cycling of phosphorus: Insights from oxygen isotope effects of phosphoenzymes. Am. J. Sci. 305, 596–620.

Butterfield, N.J., 2009. Oxygen, animals and oceanic ventilation: an alternative view. Geobiology 7, 1–7.

Byrne, R.H., Kim, K.H., 1990. Rare earth element scavenging in seawater. Geochim. Cosmochim. Acta 55, 2645–2656.

Byrne, R.H., Kim, K.H., 1993. Rare earth precipitation and coprecipitation behaviour: the limiting role of PO_4^{3-} on dissolved rare earth concentrations in seawater. Geochim. Cosmochim. Acta 57, 519–526.

Cai, Y.P., Xiao, S.H., Li, G.S., Hua, H., 2019. Diverse biomineralizing animals in the terminal Ediacaran Period herald the Cambrian explosion. Geology 47, 380–384.

Canfield, D.E., Poulton, S.W., Knoll, A.H., Narbonne, G.M., Ross, G., Goldberg, T., Strauss, H., 2008. Ferruginous conditions dominated later neoproterozoic deep-water chemistry. Science 321, 949–952.

Canfield, D.E., Poulton, S.W., Narbonne, G.M., 2007. Late-Neoproterozoic deep-ocean oxygenation and the rise of animal life. Science 315, 92–95.

Cappellen, P.V., Berner, R.A., 1988. A mathematical model for the early diagenesis of phosphorus and fluorine in marine sediments; apatite precipitation. Am. J. Sci. 288, 289–333.

Chen, J.A., Yang, R.D., Wei, H.R., Gao, J.B., 2013. Rare earth element geochemistry of Cambrian phosphorites from the Yangtze Region. J. Rare Earth. 31, 101–112.

Chen, Z.G., Huang, Y.P., Liu, G.S., Cai, Y.H., Lu, Y.Y., Liu, R., 2010. Advances in the measurement methods and fractionation mechanism of the oxygen isotope composition of phosphate. Adv. Earth Sci. 25, 1040–1050 (in Chinese with English abstract).

Colman, A.S., Blake, R.E., Karl, D.M., 2005. Marine phosphate oxygen isotopes and organic matter remineralization in the oceans. P. Natl. Acad. Sci. U.S.A. 102, 13023–13028.

Cook, P.J., 1992. Phosphogenesis around the Proterozoic Phanerozoic transition. J. Geol. Soc. 149, 615–620.

Cook, P.J., Shergold, J.H., 1984. Phosphorus, phosphorites and skeletal evolution at the Precambrian—Cambrian boundary. Nature 308, 231–236.

Coplen, T.B., Kendall, C., Hopple, J., 1983. Comparison of stable isotope reference samples. Nature 302, 236–238.

Crusius, J., Calvert, S., Pedersen, T., Sage, D., 1996. Rhenium and molybdenum enrichments in sediments as indicators of oxic, suboxic and sulfidic conditions of deposition. Earth Planet Sci. Lett. 145, 65–78.

Cunningham, J.A., Vargas, K., Yin, Z., Bengtson, S., Donoghue, P.C.J., 2017. The Weng'an Biota (Doushantuo Formation): an Ediacaran window on soft-bodied and multicellular microorganisms. J. Geol. Soc. 174, 793–802.

Delaney, M.L., 1989. Geological boundaries - extinctions and carbon cycling. Nature 337, 18–19.

Deng, K.Y., Bo, W.U., Luo, M.X., Luo, C., Long, J.X., 2015. Phosphate Rock Geochemistry of the Doushantuo Formation in Shuangshanping, Kaiyang of Guizhou Province and its Genetic Significance. Geology & Exploration 51, 123–132 (in Chinese with English abstract).

Derry, L.A., 2010. A burial diagenesis origin for the Ediacaran Shuram-Wonoka carbon isotope anomaly. Earth Planet Sci. Lett. 294, 152–162.

Dong Ye, M.X., 1996. Uppwelling oceanic curuents & Epicontinental Chi. Geology of Chemical Minerals 18, 156–162 (in Chinese with English abstract).

Elderfield, H., Pagett, R., 1986. Rare earth elements in ichthyoliths: variations with redox conditions and depositional environment. Sci. Total Environ. 49, 175–197.

Erickson, B.E., Helz, G.R., 2000. Molybdenum(VI) speciation in sulfidic waters: Stability and lability of thiomolybdates. Geochim. Cosmochim. Acta 64, 1149–1158.

Fan, H.F., Wen, H.J., Hu, R.Z., Zhang, Y.X., 2007. Stable isotope of redox-sensitive elements (Se, Cr, Mo). Earth Sci. Rev. 14, 264–276.

Fan, H.F., Wen, H.J., Zhu, X.K., 2016. Marine redox conditions in the early Cambrian ocean: insights from the lower Cambrian phosphorite deposits, South China. J. Earth Sci. 27, 282–296.

Fan, H.F., Zhu, X.K., Wen, H.J., Yan, B., Li, J., Feng, L.J., 2014. Oxygenation of Ediacaran Ocean recorded by iron isotopes. Geochim. Cosmochim. Acta 140, 80–94.

Fan, H.R., Hu, F.F., Yang, K.F., Wang, K.Y., 2005. Fluid unmixing/immiscibility as an ore-forming process in the giant REE-Nb-Fe deposit, Inner Mongolian, China: evidence from fluid inclusions. J. Geochem. Explor. 89, 104–107.

Feng, S.J., Zhao, K.D., Ling, H.F., Chen, P.R., Chen, W.F., Sun, T., Jiang, S.Y., Pu, W., 2014. Geochronology, elemental and Nd-Hf isotopic geochemistry of Devonian A-type granites in central Jiangxi, South China: Constraints on petrogenesis and post-collisional extension of the Wuyi-Yunkai orogeny. Lithos 206, 1–18.

Fike, D.A., Grotzinger, J.P., 2008. A paired sulfate-pyrite delta S-34 approach to understanding the evolution of the Ediacaran-Cambrian sulfur cycle. Geochim. Cosmochim. Acta 72, 2636–2648.

Fike, D.A., Grotzinger, J.P., Pratt, L.M., Summons, R.E., 2006. Oxidation of the Ediacaran Ocean. Nature 444, 744–747.

Filippelli, G.M., 2008. The global phosphorus cycle: past, present, and future. Elements 4, 89–95.

Filippelli, G.M., Delaney, M.L., 1992. Similar phosphorus fluxes in ancient phosphorite deposits and a modern phosphogenic environment. Geology 20, 709–712.

Föllmi, K.B., 1996. The phosphorus cycle, phosphogenesis and marine phosphate-rich deposits. Earth Sci. Rev. 40, 55–124.

Föllmi, K.B., Hosein, R., Arn, K.S., 2009. Weathering and the mobility of phosphorus in the catchments and forefields of the Rhone and Oberaar glaciers, central Switzerland: implications for the global phosphorus cycle on glacial-interglacial timescales. Geochim. Cosmochim. Acta 73, 2252–2282.
Fortier, S.M., Luttge, A., 1995. An experimental calibration of the temperature-dependence of oxygen-isotope fractionation between apatite and calcite at high-temperatures (350–800 ℃). Chem. Geol. 125, 281–290.
Fox, D., 2016. What speaked the Cambrian explosion?. Nature 530, 268–270.
Froelich, P.N., Arthur, M.A., Burnett, W.C., Deakin, M., Hensle, V., Jahnke, Y.R., Kaul, L., Kim, K.H., Roe, K., Soutar, A., Vathakanon, C., 1988. Early diagenesis of organic matter in Peru continental margin sediments: phosphorite precipitation. Mar. Geol. 80, 309–343.
Frohlich, P.N., Kim, K.H., Jahnke, R., Burnett, W.C., Soutar, A., Deakin, M., 1983. Pore water fluoride in Peru continental margin sediments: Uptake from seawater. Geochim. Cosmochim. Acta 47, 1605–1612.
Gao, S., Zhang, B.R., Wang, D.P., Ouyang, J.P., Xie, Q.L., 1996. Geochemical evidence for the Proterozoic tectonic evolution of the Qinling orogenic belt and its adjacent margins of the north China and Yangtze cratons. Precambrian Res. 80, 23–48.
Glenn, C.R., Föllmi, K.B., Riggs, S.R., Baturin, G.N., Grimm, K.A., Trappe, J., Abed, A.M., Gallioliver, C., Garrison, R.E., Ilyan, A., Jehl, C., Rohrlich, V., Sadaqah, R.M., Schidlowski, M., Sheldon, R.E., Siegmund, H., 1994. Phosphorus and phosphorites: sedimentology and environments of formation. Eclogae Geologicae Helvetiae 87, 747–788.
Goldberg, T., Strauss, H., Guo, Q., Liu, C., 2007. Reconstructing marine redox conditions for the early Cambrian Yangtze Platform: Evidence from biogenic sulphur and organic carbon isotopes. Paleogeogr. Palaeocl. 254, 175–193.
Goldhammer, T., Brunner, B., Bernasconi, S.M., Ferdelman, T.G., Zabel, M., 2011a. Phosphate oxygen isotopes: Insights into sedimentary phosphorus cycling from the Benguela upwelling system. Geochim. Cosmochim. Acta 75, 3741–3756.
Goldhammer, T., Max, T., Brunner, B., Einsiedl, F., Zabel, M., 2011b. Marine sediment pore-water profiles of phosphate $\delta^{18}O$ using are fined micro-extraction. Limnol. Oceanogr-Meth. 9, 110–120.
Govindaraju, K., 1994. Compilation of working values and sample description for 383 geostandards. Geostands Newsletter 18, 331-331.
Gruau, G., Legeas, M., Riou, C., 2005. The oxygen isotope composition of dissolved anthropogenic phosphates: a new tool for eutrophication research. Water Res. 39, 232–238.
Guilbaud, R., Slater, B.J., Poulton, S.W., Harvey, T.H.P., Brocks, J.J., Nettersheim, B.J., Butterfield, N.J., 2018. Oxygen minimum zones in the early Cambrian ocean. Geochem. Perspect. Let. 6, 33–38.
Guo, H.Y., Xia, Y., He, S., Xie, Z.J., Wei, D.T., Lei, B., 2017. Geochemical Characteristics of Zhijin Phosphorite Type Rare-earth Deposit, Guizhou Province, China. Acta Mineralogica Sinica 37, 755–763 (in Chinese with English abstract).
Guo, Q.J., Strauss, H., Liu, C.Q., Goldberg, T., Zhu, M.Y., Pi, D.H., Heubeck, C., Vernhet, E., Yang, X.L., Fu, P.Q., 2007. Carbon isotopic evolution of the terminal Neoproterozoic and early Cambrian: evidence from the Yangtze Platform, South China. Paleogeogr. Palaeocl. 254, 140–157.
Guo, Q.J., Yang, W.D., Liu, C.Q., Strauss, H., Wang, X.L., 2003. Sedimentary Geochemistry Research on the Radiation of Weng'an Biota and the Formation of the Phosphorite Ore Deposit, Guizhou. Bull. Mineral. Petrol. Geochem. 22, 11–17 (in Chinese with English abstract).
Han, T., Fan, H.F., 2015. Dynamic evolution of the Ediacaran ocean across the Doushantuo Formation, South China. Chem. Geol. 417, 261–272.
Haskin, L.A., Wildeman, T.R., Haskin, M.A., 1968. An accurate procedure for the determination of the rare earths by neutron activation. J. Radioanal. Chem. 1, 337–348.
He, T.C., Zhu, M.Y., Mills, B.J.W., Wynn, P.M., Zhuravlev, A.Y., Tostevin, R., von Strandmann, P.A.E.P., Yang, A.H., Poulton, S.W., Shields, G.A., 2019. Possible links between extreme oxygen perturbations and the Cambrian radiation of animals. Nat. Geosci. 12, 468–474.
Heggie, D.T., Skyring, G.W., Obrien, G.W., Reimers, C., Herczeg, A., Moriarty, D.J.W., Burnett, W.C., Milnes, A.R., 1990. Organic carbon cycling and modern phosphorite formation on the east Australia continental margin: An overview. In: 11th and final international field workshop and symp of international geological coffelation programme project: phosphorites. Hertford Coll, Oxford, England, pp. 87–117.
Holser, W.T., 1997. Evaluation of the application of rare-earth elements to paleoceanography. Paleogeogr. Palaeocl. 132, 309–323.
Hu, R., Wang, W., Li, S.Q., Yang, Y.Z., Chen, F.K., 2016. Sedimentary Environment of Ediacaran Sequences of South China: Trace Element and Sr-Nd Isotope Constraints. J. Jeol. 124, 769–789.
Ilyin, A.V., 1998. Rare-earth geochemistry of 'old' phosphorites and probability of syngenetic precipitation and accumulation of phosphate. Chem. Geol. 144, 243–256.
Jaisi, D.P., Blake, R.E., 2010. Tracing sources and cycling of phosphorus in Peru Margin sediments using oxygen isotopes in authigenic and detrital phosphates. Geochim. Cosmochim. Acta 74, 3199–3212.
Jaisi, D.P., Kukkadapu, R.K., Stout, L.M., Varga, T., Blake, R.E., 2011. Biotic and abiotic pathways of phosphorus cycling in minerals and sediments: insights from oxygen isotope ratios in phosphate. Environ. Sci. Technol. 45, 6254–6261.
Jarvis, I., Burnett, W.C., Nathan, Y., Almbaydin, F.S.M., Attia, A.K.M., Castro, L.N., Flicoteaux, R., Hilmy, M.E., Husain, V., Qutawnah, A.A., Serjani, A., Zanin, Y.N., 1994. Phosphorite geochemistry—state-of-the-art and environmental concern. Eclogae Geologicae Helvetiae 87, 643–700.
Jiang, G.Q., Kaufman, A.J., Christie-Blick, N., Zhang, S.H., Wu, H.C., 2007. Carbon isotope variability across the Ediacaran Yangtze platform in South China: implications for a large surface-to-deep ocean $\delta^{13}C$ gradient. Earth Planet Sci. Lett. 261, 303–320.
Jiang, G.Q., Shi, X.Y., Zhang, S.H., Wang, Y., Xiao, S.H., 2011. Stratigraphy and paleogeography of the Ediacaran Doushantuo Formation (ca. 635–551 Ma) in South China. Gondwana Res. 19, 831–849.
Jiang, G.Q., Sohl, L.E., Christieblick, N., 2003. Neoproterozoic stratigraphic comparison of the Lesser Himalaya (India) and Yangtze block (south China): Paleogeographic implications. Geology 31, 917–920.
Kaufman, A.J., Jacobsen, S.B., Knoll, A.H., 1993. The Vendian record of Sr and C isotopic variations in seawater: implications for tectonics and paleoclimate. Earth Planet Sci. Lett. 120, 409–430.
Kaufman, A.J., Knoll, A.H., 1995. Neoproterozoic varations in the C-isotope composition of seawater-stratigraphic and biogeochemical implications. Precambrian Res. 73, 27–49.
Kendall, B., Dahl, T.W., Anbar, A.D., 2017. The stable isotope geochemistry of molybdenum. Rev. Mineral. Geochem. 82, 683–732.
Knauth, L.P., Kennedy, M.J., 2009. The late Precambrian greening of the Earth. Nature 460, 728–732.
Knoll, A.H., 2000. Learning to tell Neoproterozoic time. Precambrian Res. 100, 3–20.
Knoll, A.H., Carroll, S.B., 1999. Early animal evolution: Emerging views from comparative biology and geology. Science 284, 2129–2137.
Kolodny, Y., Luz, B., Navon, O., 1983. Oxygen isotope variations in phosphate of biogenic apatites.1. Fish bone apatite-rechecking the rules of the game. Earth Planet Sci. Lett. 64, 398–404.
Institute of Geochemistry, Chinese Academy of Sciences, 1998. Higher geochemistry. Beijing Science Press, Beijing, 491 pp. (in Chinese).
Lambert, I., Walter, M., Zang, W., Lu, S.,Guo, G., M, 1987. Paleoenviroment and carbon isotope stratigraphy of Upper Proterozoic carbonates of the Yangtze Platform. Nature 325, 140-142.
Lecuyer, C., Grandjean, P., Sheppard, S.M.F., 1999. Oxygen isotope exchange between dissolved phosphate and water at temperatures ≤135°C: inorganic versus biological fractionations. Geochim. Cosmochim. Acta 63, 855–862.
Li, C., Love, G.D., Lyons, T.W., Fike, D.A., Sessions, A.L., Chu, X.L., 2010. A Stratified Redox Model for the Ediacaran Ocean. Science 328, 80–83.
Li, D.D., Zhang, X.L., Hu, D.P., Li, D., Zhang, G.J., Zhang, X., Ling, H.F., Xu, Y.L., Shen, Y. N., 2020. Multiple S-isotopic constraints on paleo-redox and sulfate concentrations across the Ediacaran-Cambrian transition in South China. Precambrian. Res. 349, 1–11.
Li, X.C., Zhou, M.F., 2018. The Nature and Origin of Hydrothermal REE Mineralization in the Sin Quyen Deposit, Northwestern Vietnam. Econ. Geol. 113, 645–673.
Liu, B.J., Xu, X.S., Luo, A.P., Kang, C.L., 1987. Storm events and phosphate deposition in Cambrian on the western margin of the Yangtze platform, China. Acta Sedimentologica Sinica 5, 28–39 (in Chinese with English abstract).
Liu, B.J., Xu, X.S., Xu, Q., Pan, X.N., Huang, H.Q., 1993. Sedimentary crustal evolution and mineralization of palaeocontinent in South China. Science Press, Beijing, 236 pp (in Chinese).
Liu, J., 2017. Mo isotopic signature of non-euxinic sediments and its paleo-oceanic significance. Ph. D. thesis, University of Chinese Academy of Sciences, 160 pp (in Chinese with English abstract).
Liang, Y.H., Blake, R.E., 2007. Oxygen isotope fractionation between apatite and aqueous-phase phosphate: 20–45 °C. Chem. Geol. 238, 121–133.
Liu, J.M., Liu, J.J., 1997. Basic fluid genetic model of sediment-hosted micro-disseminated gold deposits in the gold-triangle area between Guizhou, Guanxi and Yunnan. Acta Mineral. Sinica 17, 448–456 (in Chinese with English abstract).
Liu, Y.J., Cao, L.M., 1987. Introduction of Elemental Geochemistry Geologygal Press, Beijing, 236 pp (in Chinese).
Longinelli, A., Bartelloni, M., Cortecci, G., 1976. The isotopic cycle of oceanic phosphate. Earth Planet Sci. Lett. 32, 389–392.
Longinelli, A., Nuti, S., 1973. Revised phosphate-water isotopic temperature scale. Earth Planet Sci. Lett. 19, 373–376.
Lumiste, K., Mänd, K., Bailey, J., Paiste, P., Lang, L., Lepland, A., Kirsimäe, K., 2019. REE +Y uptake and diagenesis in Recent sedimentary apatites. Chem. Geol. 525, 268–281.
Lyons, T.W., Reinhard, C.T., Planavsky, N.J., 2014. The rise of oxygen in Earth's early ocean and atmosphere. Nature 506, 307–315.
Marshall, C. R., 2006. Explaining the Cambrian "explosion" of animals. Annu. Rev. Earth P. L. Sc. 34, 355-384.
McArthur, J. M.,Herczeg, A., 1990. Diagenetic stability of the isotopic composition of phosphate-oxygen: Palaeoenvironmental implications. In: Notholt, A.J.G and Jarvis, I. (Eds.), Phosphorite Research and Development. Geological Society Special Publicarion 52, 119-124.
McArthur, J.M., Walsh, J.N., 1984. Rare-earth geochemistry of phosphorites. Chem. Geol. 47, 191–220.
McLaughlin, K., Cade-Menun, B.J., Paytan, A., 2006. The oxygen isotopic composition of phosphate in Elkhorn Slough, California: A tracer for phosphate sources. Estuar. Coast. Shelf Sci. 70, 499–506.
Mi, W.T., 2010. The sequence stratigraphy and genesis of phosphorites of doushantuo formation at Baiguoyuan, Yichang, Hubei. Acta Sedimentol. Sinica 30, 471–480 (in Chinese with English abstract).
Mizota, C., Domon, Y., Yoshida, N., 1992. Oxygen isotope composition of natural phosphates from volcanic ash soils of the Great Rift Valley of Africa and east Java, Indonesia. Geoderma 53, 111–123.

Morad, S., Felitsyn, S., 2001. Identification of primary Ce-anomaly signatures in fossil biogenic apatite: implication for the Cambrian oceanic anoxia and phosphogenesis. Sediment. Geol. 143, 259–264.
Morford, J.L., Emerson, S., 1999. The geochemistry of redox sensitive trace metals in sediments. Geochim. Cosmochim. Acta 63, 1735–1750.
Murray, R.W., Tenbrink, M.R.B., Jones, D.L., Gerlach, D.C., Russ, G.P., 1990. Rare earth elements as indicators of different marine depositional enviornments in cherts and shale. Geology 18, 268–271.
Muscente, A.D., Hawkins, A.D., Xiao, S., 2015. Fossil preservation through phosphatization and silicification in the Ediacaran Doushantuo Formation (South China): a comparative synthesis. Paleogeogr. Palaeocl. 434, 46–62.
Nägler, T.F., Anbar, A.D., Archer, C., Goldberg, T., Gordon, G.W., Greber, N.D., Siebert, C., Sohrin, Y., Vance, D., 2014. Proposal for an international molybdenum isotope measurement standard and data representation. Geostand. Geoanal. Res. 38, 149–151.
Nägler, T.F., Neubert, N., Böttcher, M.E., Dellwig, O., Schnetger, B., 2011. Molybdenum isotope fractionation in pelagic euxinia: Evidence from the modern Black and Baltic Seas. Chem. Geol. 289, 1–11.
Noordmann, J., Weyer, S., Montoya-Pino, C., Dellwig, O., Neubert, N., Eckert, S., Paetzele, M., Böttcher, M.E., 2015. Uranium and molybdenum isotope systematics in modern euxinic basins: case studies from the central Baltic Sea and the Kyllaren fjord (Norway). Chem. Geol. 396, 182–195.
Och, L.M., Shields-Zhou, G.A., 2012. The Neoproterozoic oxygenation event: environmental perturbations and biogeochemical cycling. Earth Sci. Rev. 110, 26–57.
Paul, S.A.L., Volz, J.B., Bau, M., Koster, M., Kasten, S., Koschinsky, A., 2019. Calcium phosphate control of REY patterns of siliceous-ooze-rich deep-sea sediments from the central equatorial Pacific. Geochim. Cosmochim. Acta 251, 56–72.
Paytan, A., Kolodny, Y., Neori, A., 2002. Rapid biologically mediated oxygen isotope exchange between water and phosphate. Global Biogeochem. Cycl. 16, 855–862.
Planavsky, N.J., Rouxel, O.J., Bekker, A., Lalonde, S.V., Konhauser, K.O., Reinhard, C.T., Lyons, T.W., 2010. The evolution of the marine phosphate reservoir. Nature 467, 1088–1090.
Pourret, O., Davranche, M., Gruau, G., Dia, A., 2008. New insights into cerium anomalies in organic-rich alkaline waters. Chem. Geol. 251, 120–127.
Pufahl, P.K., Grimm, K.A., 2003. Coated phosphate grains: Proxy for physical, chemical, and ecological changes in seawater. Geology 31, 801–804.
Pufahl, P.K., Groat, L.A., 2017. Sedimentary and igneous phosphate deposits: formation and exploration: an invited Paper. Econ. Geol. 112, 483–516.
Pufahl, P.K., Hiatt, E.E., 2012. Oxygenation of the Earth's atmosphere-ocean system: a review of physical and chemical sedimentologic responses. Mar. Petrol. Geol. 32, 1–20.
Qi, L., Hu, J., Gregoire, D.C., 2000. Determination of trace elements in granites by inductively coupled plasma mass spectrometry. Talanta 51, 507.
Reinhard, C.T., Planavsky, N.J., Gill, B.C., Ozaki, K., Robbins, L.J., Lyons, T.W., Fischer, W.W., Wang, C., Cole, D.B., Konhauser, K.O., 2017. Evolution of the global phosphorus cycle. Evolution of the global phosphorus cycle 541, 386–389.
Reynard, B., Lécuyer, C., Grandjean, P., 1999. Crystal-chemical controls on rare-earth element concentrations in fossil biogenic apatites and implications for paleoenvironmental reconstructions. Chem. Geol. 155, 233–241.
Riggs, S.R., 1979. Phosphorite sedimentation in Florida—a model phosphogenic system. Econ. Geol. 74, 285–314.
Rudnick, R., Gao, S., 2003. Composition of the continental crust. Treatise on Geochemistry 3, 659.
Ruttenberg, K.G., Berner, R.A., 1993. Authigenic apatite formation and burial in sediments from non-upwelling, continental margin environments. Geochim. Cosmochim. Acta 57, 991–1007.
Shaffer, G., 1986. Phosphate pumps and shuttles in the Black Sea. Nature 321, 515–517.
She, Z.B., Strother, P., McMahon, G., Nittler, L.R., Wang, J.H., Zhang, J.H., Sang, L.K., Ma, C.Q., Papineau, D., 2013. Terminal Proterozoic cyanobacterial blooms and phosphogenesis documented by the Doushantuo granular phosphorites I: In situ micro-analysis of textures and composition. Precambrian Res. 235, 20–35.
She, Z.B., Strother, P., Papineau, D., 2014. Terminal Proterozoic cyanobacterial blooms and phosphogenesis documented by the Doushantuo granular phosphorites II: Microbial diversity and C isotopes. Precambrian Res. 251, 62–79.
Shemesh, A., Kolodny, Y., Luz, B., 1988. Isotope geochemistry of oxygen and carbon in phosphate and carbonate of phosphorite francolite. Geochim. Cosmochim. Acta 52, 2565–2572.
Shen, Y.N., Zhao, R., Chu, X.L., Lei, J.J., 1998. The carbon and sulfur isotope signatures in the Precambrian-Cambrian transition series of the Yangtze Platform. Precambrian Res. 89, 77–86.
Shi, C.H., 2005. Formation of phosphorite deposit, Breakup of Rodinia supercontinent and Biology explosion- A case study of Weng'an, Kaiyang and Zhijin phosphorite deposits of Guizhou Province. Ph. D. thesis, University of Chinese Academy of Sciences, 108 pp (in Chinese with English abstract).
Shi, C.H., Hu, R.Z., Wang, G.Z., 2004. Study on REE geochemistry of Zhijin phosphorites, Guizhou province. Jmineral Report 24, 71–75 (in Chinese with English abstract).
Shields, G., Stille, P., 2001. Diagenetic constraints on the use of cerium anomalies as palaeoseawater redox proxies: an isotopic and REE study of Cambrian phosphorites. Chem. Geol. 175, 29–48.
Shimizu, H., Masuda, A., 1977. Cerium in chert as an indication of marine environment of its formation. Nature 266, 346–348.
Shimura, T., Kon, Y., Sawaki, Y., Hirata, T., Han, J., Shu, D.G., Komiya, T., 2014. In-situ analyses of phosphorus contents of carbonate minerals: Reconstruction of phosphorus contents of seawater from the Ediacaran to early Cambrian. Gondwana Res. 25, 1090–1107.
Shu, L.S., 2012. An analysis of principal features of tectonic evolution in South China Block. Geol. Bull. China 31, 1035–1053 (in Chinese with English abstract).
Siebert, C., Nägler, T.F., von Blanckenburg, F., Kramers, J.D., 2003. Molybdenum isotope records as a potential new proxy for paleoceanography. Earth Planet Sci. Lett. 211, 159–171.
Soudry, D., 1992. Primary bedded phosphorites in the Campanian Mishash Formation, Negev, southern Israel. Sediment. Geol. 80, 77–88.
Sperling, E.A., Stockey, R.G., 2018. The Temporal and Environmental Context of Early Animal Evolution: Considering All the Ingredients of an "Explosion". Integr. Comp. Biol. 58, 605–622.
Stammeier, J.A., Hippler, D., Nebel, O., Leis, A., Grengg, C., Mittermayr, F., Kasemann, S.A., Dietzel, M., 2019. Radiogenic Sr and Stable C and O Isotopes Across Precambrian-Cambrian Transition in Marine Carbonatic Phosphorites of Malyi Karatau (Kazakhstan)-Implications for Paleo-environmental Change. Geochem. Geochem. Geosy. 20, 3–23.
Steiner, M., Wallis, E., Ertman, B.D., Zhao, Y.L., Yang, R.D., 2001. Submarine hydrothermal exhalative ore layers in black shales from South China and associated fossils insights into Lower Cambrian facies and bio-evolution. Paleogeogr. Palaeocl. 169, 165–169.
Stout, L.M., Joshi, S.R., Kana, T.M., Jaisi, D.P., 2014. Microbial activities and phosphorus cycling: an application of oxygen isotope ratios in phosphate. Geochim. Cosmochim. Acta 138, 101–116.
Taylor, R.P., 1992. Petrological and geochemical characteristics of the Pleasant Ridge zinnwaldite-topaz granite, southern New Brunswick, and comparisons with other topaz-bearing felsic rocks. In: Workshop on the mineralogy, geochemistry and petrology of granitic pegmatites. University of Maniboba, Winnipeg, Canada, pp. 895–921.
Taylor, S.R., Mclennan, S.M., 1985. The Continental Crust: Its Composition and Evolution, An Examination of the Geochemical Record Preserved in Sedimentary Rocks. Scientific Publications, Oxford, Blackwell, pp. 1–312.
Tossell, J.A., 2005. Calculating the partitioning of the isotopes of Mo between oxidic and sulfidic species in aqueous solution. Geochim. Cosmochim. Acta 69, 2981–2993.
Veevers, J.J., 2004. Gondwanaland from 650–500 Ma assembly through 320 Ma merger in Pangea to 185–100 Ma breakup: supercontinental tectonics via stratigraphy and radiometric dating. Earth Sci. Rev. 68, 1–132.
Voegelin, A.R., Nägler, T.F., Samankassou, E., Villa, I.M., 2009. Molybdenum isotopic composition of modern and Carboniferous carbonates. Chem. Geol. 265, 488–498.
Walter, M.R., Veevers, J.J., Calver, C.R., Gorjan, P., Hill, A.C., 2000. Dating the 840–544 Ma Neoproterozoic interval by isotopes of strontium, carbon, and sulfur in seawater, and some interpretative models. Precambrian Res. 100, 371–433.
Wang, J., Li, Z.X., 2003. History of Neoproterozoic rift basins in South China: implications for Rodinia break-up. Precambrian Res. 122, 141–158.
Wang, X.,Q., 2010. Organic carbon isotope evidence for late Ediacaran – early Cambrian ocean stratification in South China. Ph. D. thesis, China University of Geosciences (Beijing), 101 pp (in English with Chinese and English abstract).
Wang, Y.L., Liu, Y.L., Schimitt, A.A., 1986. Rare eatrh element geochemistry of south Atlantic deep sea sediments: Ce anomaly change approximately – 54 My. Geochim. Cosmochim. Acta 50, 1337–1355.
Wang, Z.P., Zhang, Y.G., Du, Y.S., Chen, G.Y., Liu, J.Z., Xu, Y.Y., Tan, D., W.,, Li, L., Wang, D.F.,Wu, W.M., 2016. Reconstruction of quantitative lithofacies palaeogeography of the Sinian Doushantuo Age of phosphorite depositional zone in Kaiyang area, central Guizhou Province. Journal of Palaeogeography 18, 399-410 (in Chinese with English abstract).
Wei, G.Y., Ling, H.F., Shields, G.A., Chen, T.Y., Lechte, M., Chen, X., Qiu, C., Lei, H.L., Zhu, M.Y., 2019. Long-term evolution of terrestrial inputs from the Ediacaran to early Cambrian: Clues from Nd isotopes in shallow-marine carbonates, South China. Palaeogeography, Palaeoclimatology, Palaeoecology 535, 1–12.
Wei, G.J., Ma, J.L., Liu, Y., Xie, L.H., Lu, W.J., Deng, W.F., Ren, Z.Y., Zeng, T., Yang, Y.H., 2013. Seasonal changes in the radiogenic and stable strontium isotopic composition of Xijiang River water: implications for chemical weathering. Chem. Geol. 343, 67–75.
Wen, H.J., Carignan, J., Zhang, Y.X., Fan, H.F., Cloquet, C., Liu, S.R., 2011. Molybdenum isotopic records across the Precambrian-Cambrian boundary. Geology 39, 775–778.
Wen, H.J., Zhang, Y.X., Fan, H.F., Hu, R.Z., 2010. Mo isotopes in the Lower Cambrian formation of southern China and its implications on paleo-ocean environment. Chin. Sci. Bull. 54, 4756–4762 (in Chinese with English abstract).
Wille, M., Nagler, T.F., Lehmann, B., Schroder, S., Kramers, J.D., 2008. Hydrogen sulphide release to surface waters at the Precambrian/Cambrian boundary. Nature 453, 767–769.
Wood, S.A., Shannon, W.M., 2002. Rare-earth elements in geothermal waters from Oregon, Nevada, and California. J. Solid. State Chem. 171, 246–253.
Wu, K., Ma, D.S., Pan, J.Y., Nie, W.M., Zhou, J., Xia, F., Liu, L., 2006. The Geochemistry of phosphorite of Doushantuo formation in Weng'an, China: insights from trace elements and REE. J. East China Inst. Technol. 29, 108–114 (in Chinese with English abstract).
Wu, X.H., Han, Z.J.,Cai, J.F., 1999. Guizhou phosphorite. Geological Publishing House, Beijing, 339 pp (in Chinese).
Xiao, S.H., Knoll, A.H., 1999. Fossil preservation in the Neoproterozoic Doushantuo phosphorite Lagerstatte, South China. Lethaia 32, 219–240.

Xiao, S.H., Knoll, A.H., 2000. Phosphatized animal embryos from the Neoproterozoic Doushantuo Formation at Weng'An, Guizhou, South China. J. Palaeogeog. 74, 767–788.
Xiao, S.H., Zhang, Y., Knoll, A.H., 1998. Three-dimensional preservation of algae and animal embryos in a Neoproterozoic phosphorite. Nature 391, 553–558.
Xie, Q.L., Chen, D.F., Qi, L., Chen, X.P., 2003. Ree geochemistry of doushantuo phosphorites and paleoenvironmental changes in weng'an area, south China. Acta Mineral. Sinica 23, 289–295 (in Chinese with English abstract).
Xin, H., Jiang, S.Y., Yang, J.H., Wu, H.P., Pi, D.H., 2015. Rare earth element and Sr–Nd isotope geochemistry of phosphatic rocks in Neoproterozoic Ediacaran Doushantuo Formation in Zhangcunping section from western Hubei Province. South China. Paleogeogr. Palaeocl. 440, 712–724.
Xue, Y.S., Cao, R.J., Tang, T.F., Yin, L.M., Yu, C.L., Yang, J.D., 2001. The Sinian stratigraphic sequence of the Yangtze region and correlation to the late Precambrian strata of North China. J. Stratigraphy 25, 207–216+234 (in Chinese with English abstract).
Yang, H.Y., Xiao, J.F., Xia, Y., Xie, Z.J., Tan, Q.P., Xu, J.B., Guo, H.Y., He, S., Wu, S.W., 2019. Origin of the Ediacaran Weng'an and Kaiyang phosphorite deposits in the Nanhua basin, SW China. J. Asian Earth Sci. 182, 1–24.
Yang, J.D., Sun, W.G., Wang, Z.Z., Xue, Y.S., Tao, X.C., 1999. Variations in Sr and C isotopes and Ce anomalies in successions from China: evidence for the oxygenation of Neoproterozoic seawater? Precambrian Res. 99, 215–233.
Yang, W.D., Xiao, J.K., Yu, B.S., Fang, T., Chen, F., Lu, X.Y., 1997. The sedimentology, geochemistry and sustainable Development strategies of Yunnan and Guizhou phosphorite. Geological Publishing House, Beijing, pp. 1–106 (in Chinese).
Ye, L.J., 1989. Chinese phosphorite rock. Science Press, Beijing, 339 pp (in Chinese).
Yin, K.H., Jin, H.Y., Ye, D.S., Zhu, C.L., 2007a. Geologic feature and sedimentary environment of upper Sinian Mofang phosphorite deposit in Fuquan. Geology of Chemical Minerals 29, 215–221 (in Chinese with English abstract).
Yin, L., Zhu, M., Knoll, A. H., Yuan, X., Zhang, J.,Hu, J., 2007. Doushantuo embryos preserved inside diapause egg cysts. Doushantuo embryos preserved inside diapause egg cysts 446, 661-663.
You, J.F., Wu, D.X., Liu, H.Q., 1986. Electrochemical studies of molybdate and thiomolybdates. Polyhedron 5, 535–537.
Young, M.B., McLaughlin, K., Kendall, C., 2009. Characterizing the oxygen isotopic composition of phosphate sources to aquatic ecosystems. Environ. Sci. Technol. 43, 5190–5196.
Yuan, H.Z., Li, Q., Kukkadapu, R.K., Liu, E., Yu, J.H., Fang, H., Li, H., Jaisi, D.P., 2019. Identifying sources and cycling of phosphorus in the sediment of a shallow freshwater lake in China using phosphate oxygen isotopes. Sci. Total Environ. 676, 823–833.
Zazzo, A., Lecuyer, C., Mariotti, A., 2004. Experimentally-controlled carbon and oxygen isotope exchange between bioapatites and water under inorganic and microbially-mediated conditions. Geochim. Cosmochim. Acta 68, 1–12.
Zhang, G.W., Li, S.Z., Dong, Y.P., Liu, S.F., He, D.F., Cheng, S.Y., Lu, R.K., Yao, A.P., 2013. Structure and the problems of the South China continent. Chin. Sci. Bull. 3, 1553–1582 (in Chinese with English abstract).
Zhang, J., Amakawa, H., Nozaki, Y., 1994. The comparative behaviors of Yttrium and Lanthanides in the seawater of the North Pacfic. Geophys. Res. Lett. 21, 2677–2680.
Zhang, J., Zhang, Q., Chen, D.L., 2003. REE geochemistry of the Ore-bearing REE in Xinhua phosphorite, Zhijin, Guizhou. J. Mineral. Petrol. 3, 35–38.
Zhang, J., Zhang, Q., Chen, D.L., 2004. REE geochemistry of the Xinhua REE – bearing phosphorite deposit, Zhijin County, Guizhou Province. Geology and Prospecting 40, 40–44 (in Chinese with English abstract).
Zhang, X.L., Shu, D.G., Han, J., Zhang, Z.F., Liu, J.N., Fu, D.J., 2014. Triggers for the Cambrian explosion: hypotheses and problems. Gondwana Res. 25, 896–909.
Zhang, Y.G., Du, Y.S., Chen, G.Y., Liu, J.Z., Wang, Z.P., Xu, Y.Y., Tan, D.W., Li, L., Wang, D.F., Wu, W.M., 2016. Sedimentary characteristics and mineralization model of high-grade phosphorite in the Sinian Doushantuo Age of Kaiyang area, central Guizhou Province. J. Palaeogeog. 18, 581–594.
Zhang, Y.G., Pufahl, P.K., Du, Y.S., Chen, G.Y., Liu, J.Z., Chen, Q.G., Wang, Z.P., Yu, W.C., 2019. Economic phosphorite from the Ediacaran Doushantuo Formation, South China, and the Neoproterozoic-Cambrian Phosphogenic Event. Sediment. Geol. 388, 1–19.
Zhang, Y.X., Wen, H.J., Fan, H.F., 2009. Chemical pretreatment methods for measurement of Mo isotope ratioon geological samples. Chin. J. Anal. Chem. 37, 216–220 (in Chinese with English abstract).
Zhao, L.S., Chen, Z.Q., Algeo, T.J., Chen, J., Chen, Y., Tong, J., Gao, S., Zhou, L., Hu, Z., Liu, Y.S., 2013. Rare-earth element patterns in conodont albid crowns: evidence for massive inputs of volcanic ash during the latest Permian biocrisis?. Global. Planet. Change 105, 135–151.
Zhou, C.M., Xie, G.W., McFadden, K., Xiao, S.H., Yuan, X.L., 2007. The diversification and extinction of Doushantuo-Pertatataka acritarchs in South China: causes and biostratigraphic significance. Geol. J. 42, 229–262.
Zhu, B., Jiang, S.Y., 2017. LA-ICP-MS analysis of rare earth elements on phosphatic grains of the Ediacaran Doushantuo phosphorite at Weng'an, South China: implication for depositional conditions and diagenetic processes. Geol. Mag. 154, 1381–1397.
Zhuravlev, A.Y., Wood, R.A., 2018. The two phases of the Cambrian Explosion. Sci. Rep. 8, 1–10.